Nanoscale

Accepted Manuscript

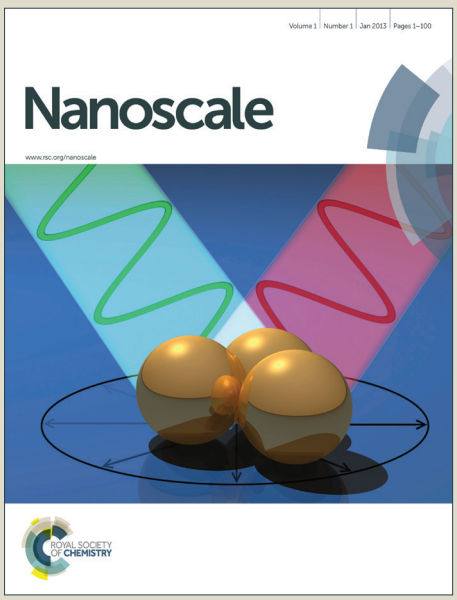

ROYAL SOCIETY OF CHEMISTRY

www.rsc.org/nanoscale

Recent Developments in 2D Layered Inorganic Nanomaterials for Sensing

Padmanathan Karthick Kannan,[1] Dattatray J. Late,[2] Hywel Morgan[3,*] and Chandra Sekhar Rout,[1,*]

[1]*School of Basic Sciences, Indian Institute of Technology Bhubaneswar, Bhubaneswar 751013, India*

[2]*Physical & Materials Chemistry Division, CSIR-National Chemical Laboratory, Dr. Homi Bhabha Road, Pashan, Pune 411008, India*

[3]*School of Electronics and Computer Science, University of Southampton, Southampton SO17 1BJ, United Kingdom*

ABSTRACT

Two dimensional layered inorganic nanomaterials (2D-LIN) have recently attracted huge interest because of their unique thickness dependent physical and chemical properties and potential technological applications. The properties of these layered materials can be tuned *via* both various physical and chemical processes. Some 2D layered inorganic nanomaterials like MoS_2, WS_2 and SnS_2 have been recently developed and employed in various applications, including new sensors because of their layer-dependent electrical properties. This article presents a comprehensive overview of recent developments in the application of 2D layered inorganic nanomaterials for sensors. Some of the salient features of 2D materials for different sensing applications are discussed, including gas sensing, electrochemical, SERS and biosensing, SERS sensors and photodetection. The working principles of the sensors are also discussed together examples.

Corresponding Author Email address: csrout@iitbbs.ac.in (C.S.R), hm@ecs.soton.ac.uk (H.M).

1. Introduction

Graphene, a 2D layered carbon nanomaterial has been the subject of intense interest because of its attractive and exceptional physical and chemical properties. Over the past few years, numerous attempts have been made to develop graphene-based devices with unique electronic, optoelectronic, electrochemical and biomedical applications[1–7]. Several excellent review articles [1–7]and books [8–10] highlight the preparation and potential application of graphene. Although a lot of attention has focused on the synthesis and application of graphene[11], recently alternative 2D layered inorganic nanomaterials (2D-LIN) have attracted attention, as new and novel inorganic layered materials with interesting physical and chemical properties. Examples of such 2D inorganic nanomaterials include hexagonal boron nitride (h-BN), molybdenum disulphide (MoS_2), tungsten disulphide (WS_2), indium selenide (In_2Se_3), gallium selenide (GaSe), vanadium selenide (VSe_2), iron sulphide (FeS), tungsten selenide (WSe_2), molybdenum selenide ($MoSe_2$), gallium telluride (GaTe), gallium sulphide (GaS). Applications of 2D-LIN for novel electronic devices such as electrochemical sensors, biosensors, solar cells, gas sensors, field emitters, FETs etc. have recently been reported [12–17]. Fig. 1 displays examples of some of these materials together with a range of technological applications.

Recent reviews on 2D-LIN have discussed synthesis, properties and their applications in various fields, such as gas and electrochemical sensors, FET biosensors, gas adsorption and storage, supercapacitors, lithium ion and sodium batteries, oxygen reduction and hydrogen evolution reaction, and superconducting properties [18–26]. This review focuses on recent developments in the field of 2D-LIN and their application to sensing.

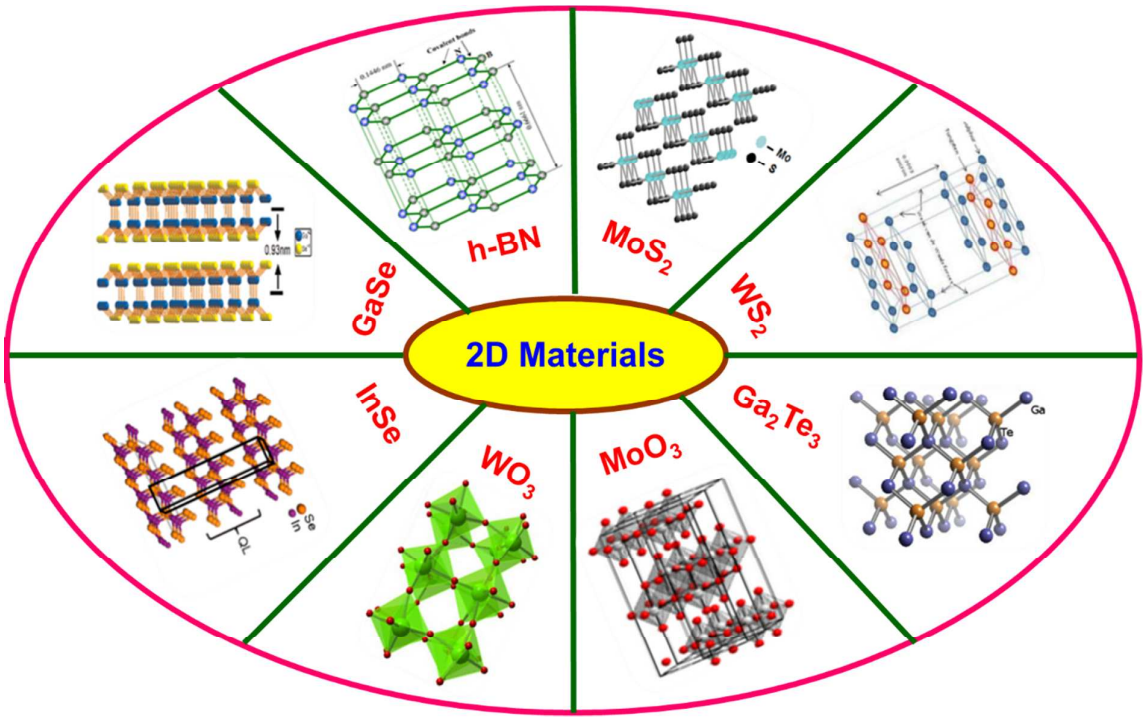

Fig. 1 Examples of inorganic 2D materials

We first discuss methods for synthesizing and preparing novel 2D-LIN along with the working principles of the sensors. We also describe salient features of the nanomaterials together with graphene and carbon nanotube (CNT) nanocomposites. The review covers the use of 2D-LIN in sensing.

2. Synthesis

A variety of methods have been employed in the preparation of 2D inorganic nanomaterials and Fig. 2 describes the range of approaches that have been adapted and developed for the synthesis of the nanomaterials. Micromechanical exfoliation (Scotch-tape method) is the simplest and the traditional technique used for the preparation of atomically thin layers of 2D nanomaterials with high quality and crystallinity. Novoselov *et al.* first applied the exfoliation method in the preparation of graphene from bulk graphite material [27]. Since then there have been extensive reports on the use of exfoliation for the preparation of other 2D inorganic nanomaterials like h-BN, WS_2, MoS_2 and In_2Se_3 [28–31]. Techniques like optical microscopy, AFM, FESEM and HRTEM can be used to identify the number of layers Mono and multi layers of 2D nanomaterials prepared by exfoliation are widely used in FET transistor and photo detector applications[32–34]. However, large scale production of materials is not possible by this method, which is one of the major limitations of the technique. In addition to micro-mechanical cleavage, pulsed laser deposition (PLD) has also been used to prepare thin films of layered 2D inorganic nanomaterials on suitable substrates, where laser pulses are used to ablate the bulk target material. The spot size and energy density of the laser beam, ablation time, irradiation angle,

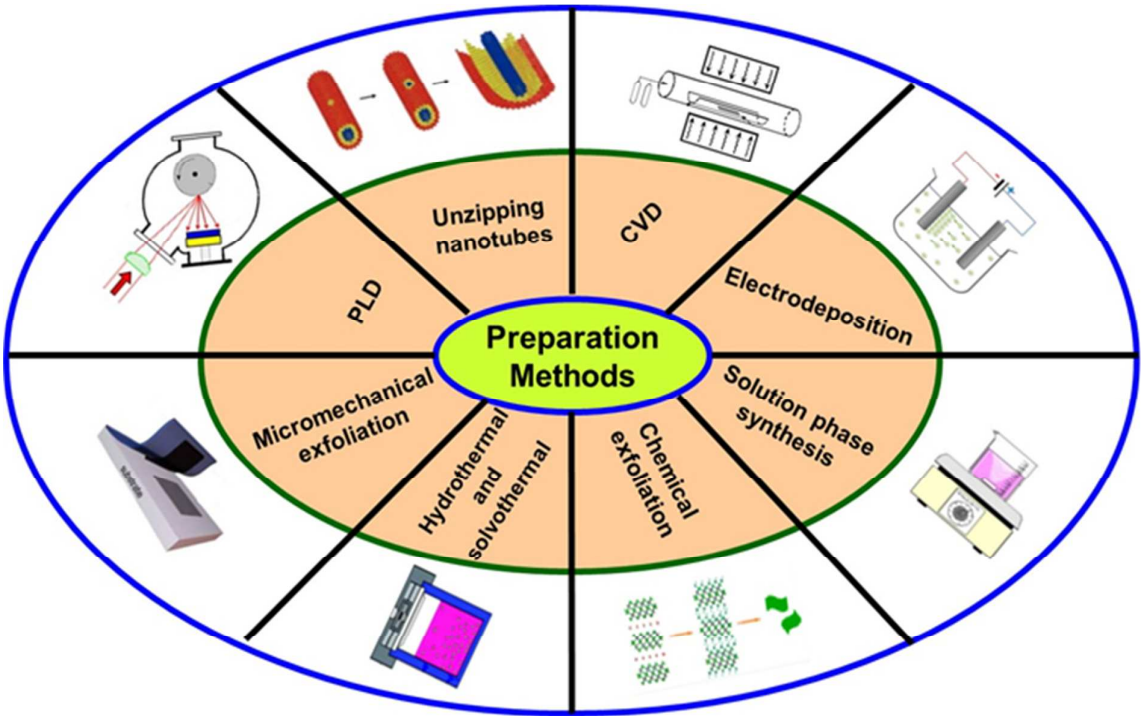

Fig. 2 The range of synthetic approaches used to fabricate 2D layered inorganic nanomaterials

substrate temperature and chamber vacuum are parameters that determine the quality of the deposited thin films[35,36]. Recently, unzipping has emerging as an efficient technique for the synthesis of 2D layered nanostructures. Jiao *et al.* and Kosynkin *et al.* successfully employed this technique for the first time to prepare graphene nanosheets from MWCNTs [37,38]. Since then, many reports have appeared on the preparation of graphene nanosheets from MWCNTs [39–43]. Besides chemical unzipping, plasma, microwave, electrochemical, microwave and laser assisted unzipping methods have all been used to prepare graphene nanosheets [44–47]. Very recently, this method has been explored for preparing BN and WS_2 nanosheets. Hydrothermal and solvothermal methods have also been extensively employed to prepare 2D-LINs.. Many reports have appeared in the literature for the preparation of 2D-LIN such as MoS_2, WS_2, SnS, VS_2, CoS_2 by hydrothermal and solvothermal methods[48–58]. Liquid exfoliation is the simplest method for large scale production. In this method, commercially available or synthesized samples are sonicated in an aqueous or non-aqueous medium for a long period of time (e.g. 3 to 8 h) to produce layered nanostructures. Organic compounds like dimethyl formamide[59], N-methyl pyrrolidone[60], methanesulfonic acid[61], chloroform-acetonitrile mixture[62], ethanol-water mixture[63], and 1-dodecyl-2-pyrrolidinone[64] are used as solvents. During sonication, the van der Waals interactions are broken yielding single or few layers of materials like WS_2. Solution phase synthesis is a chemical method in which large quantities of layered inorganic nanomaterials can be easily synthesized. CVD is a practical method for scalable and reproducible synthesis of large-area, high-quality 2D materials with a thickness of single or few atomic layers. Atmospheric pressure chemical vapour deposition has been recently used for the deposition of scalable large area nanoscale MoS_2 thin films on substrates such as sapphire, SiO_2/Si and c-axis ZnO. Electrochemical deposition is a viable technique for the preparation of thin films of nanomaterials in a reproducible and controlled manner. The thickness and properties of the material to be deposited can be tuned by varying the time,

current and potential. Other metal chalcogenides like WS_2, FeS_2, CuS, SnS and $CuInS_2$ have also been prepared using electrochemical methods[65–69]. Although there are reports on the preparation of 2D inorganic materials by electrodeposition, it remains a major challenge to prepare these 2D materials with high quality and reproducibility. Similar to hydrothermal and solvothermal method, the ionothermal method is considered to be a more eco-friendly and safer. Water soluble room temperature ionic liquids are used as solvents and these liquids have some advantageous properties such as low vapour pressure, high thermal stability and tunable solubility.

3 Applications of 2D-LIN for sensing

3.1 Gas sensors

3. 1.1 Sensing mechanisms

Most of the 2D-LIN gas sensors reported to date are based on the chemiresistive technique. Generally, upon exposure to reactive gases the gaseous species are adsorbed on the surface of the sensing material, changing the resistance of the active material due to the surface interactions and charge transfer processes. When the sensor is again exposed to air (or an inert environment), the gas molecules desorb from the sensor surface and the sensor regains its original resistance. The performance of these chemiresistive sensors are characterized by various parameters. Some of the measurands are sensor response, sensitivity, response and recovery time, selectivity and stability. The sensor response S (%) is defined as the ratio between the change in resistance value of the sensor in the presence and absence of gas molecules with respect to the initial resistance of the sensor:

$$S\ (\%) = \left[\frac{R_g - R_{air}}{R_{air}}\right] \times 100 \quad (1)$$

Where R_{air} is the resistance of the sensor in air and R_g is the resistance of the sensor in the presence of target gas. Sensitivity (S) can also be defined as the change of measured signal

per analyte concentration unit. Normally, this value can be extracted from the slope of a calibration plot, i.e. a plot of concentration vs. sensor response. Another important parameter is the response and recovery time, which is a key performance indicator for gas sensors. The response time is defined as the time taken to reach 90% of the full response after a stimulus. The recovery time is the opposite, the time taken to return to 90 % after the stimulus is removed. Selectivity measures the response to a specific group of analytes or even to a single analyte. Stability is an important measurand which characterises the quality of a signal over time.

All of these sensor parameters are strongly dependent on the sensing material. Over the past decades nanostructured metal oxides and conducting polymers have been widely employed for gas sensing[70–72]. However, in recent years, carbon nanotubes and graphene have attracted considerable attention as gas sensors because of their porous structure and high surface to volume ratio[73,74]. Since the surface area of these samples is very large, the adsorption of gas molecules is very high which improves the sensitivity and kinetics of sensing. Recently, the development of new 2D-LIN has opened up new avenues in gas sensors because of their high electrical conductivity and large surface area compared to conventional nano metal oxides. Most of the reported 2D-LIN gas sensors are simple chemiresistive FETs that have low power consumption can be easily fabricated. Classical gas sensing theory cannot be applied to these materials as the mechanism responsible for sensing is the charge transfer reaction between the adsorbed gaseous species and sensing surface, whereas in conventional metal oxide based gas sensors, surface adsorbed oxygen plays a vital role. Although there are reports describing the use of 2D-LIN as gas sensors, the sensing mechanism is still to be thoroughly investigated. Zhou and his group demonstrated the sensing performance of MoS_2 FET towards NO_2 (nitrogen di-oxide) and NH_3 (ammonia)[75]. They explained the sensing mechanism of an MoS_2 FET sensor as a charge transfer reaction

between adsorbed gaseous species and the sensor surface. It is well known that NO_2 and NH_3 are oxidizing and reducing gases respectively. When the FET sensor device is exposed to NO_2, the concentration of electrons in the conduction band of the MoS_2 is decreased because of the electron withdrawing property of NO_2. Therefore, a larger positive potential is required for operation and the device exhibits a positive shift in threshold voltage with increasing NO2, as shown in Figure 3a. Similarly, when the device is exposed to NH_3, the electron concentration is increased in the device and a lower voltage is required to turn on the device. The sensor therefore shows a negative shift for NH_3 gas (Figure 3a). These observations demonstrate that working principle of the MoS_2 based gas sensors is the change in carrier concentration due to charge transfer processes (Figure 3b). In a similar study by Cho and his group, the NO_2 and NH_3 sensing properties of MoS_2 prepared by CVD was demonstrated with a simple chemiresistive sensor[76]. The working mechanism of this gas sensor was elucidated as charge a transfer mechanism using *in situ* photo-luminescence (PL) spectroscopy and density functional theory. More specifically, when the sensor was exposed to an oxidizing gas like NO_2, the intensity of the A^+ peak in the PL spectrum increased while the A^0 peak decreased. This is because of the generation of more holes due to extraction of electron from the MoS_2 by NO_2. Opposite trends were observed for NH_3, due to the increase of neutral excitons caused by the dissociation of positive trions from the neutral excitons. This *in situ* PL study clarified the charge transfer processes between adsorbed gaseous species and MoS_2. A schematic diagram of the sensing mechanism of MoS_2 sensors in the presence and absence of analyte gases and the corresponding *in situ* PL data is shown in Fig. 3c.

3.1.2 Current status

Gas sensors have potential applications in many fields such as environmental monitoring, outdoor air quality, process control and safety, medical diagnostics etc.[77]. Over

the past few years, many materials have been developed for gas sensing, including nanostructured metals and metal oxides, nano conducting polymers, carbon nanotubes and their nanocomposites[74,78–82]. Recently, graphene has attracted attention because of its high surface to volume ratio. A material with high surface area can exhibit good sensitivity and selectivity with a short response and fast recovery time. Compared to traditional metal oxide based gas sensors, graphene exhibits superior sensing performance[83]. In addition to good surface to volume ratio, another important property for a gas sensing material is its semiconductivity because, upon exposure to gas molecules, the transport characteristics of an active material will be modulated giving enhanced sensor performance[84]. Based on this aspect, graphene fails as it has zero band gap. Also, there is a great demand to develop cost effective gas sensors with high sensitivity and low power consumption. In order to overcome these problems it is essential to develop novel 2D layered materials like graphene but with band gaps suitable for gas sensing. In case of 2D materials not only the "semiconductivity" property but also other properties such as enhanced catalytic properties, high surface area, active sites and reactivity plays important role for its sensing performance. Many 2D layered inorganic materials have now been developed, including MoS_2, WS_2, WSe_2, GaS, $GaSe_2$, FeS_2, CuS, $NdSe_2$ and h-BN, but only a few material such as MoS_2 have been used as gas sensors. MoS_2 is an n type semiconductor with a band gap of 1.2 eV. Unlike graphene, bulk MoS_2 possesses a large band gap, which becomes wider and direct (1.9 eV) for

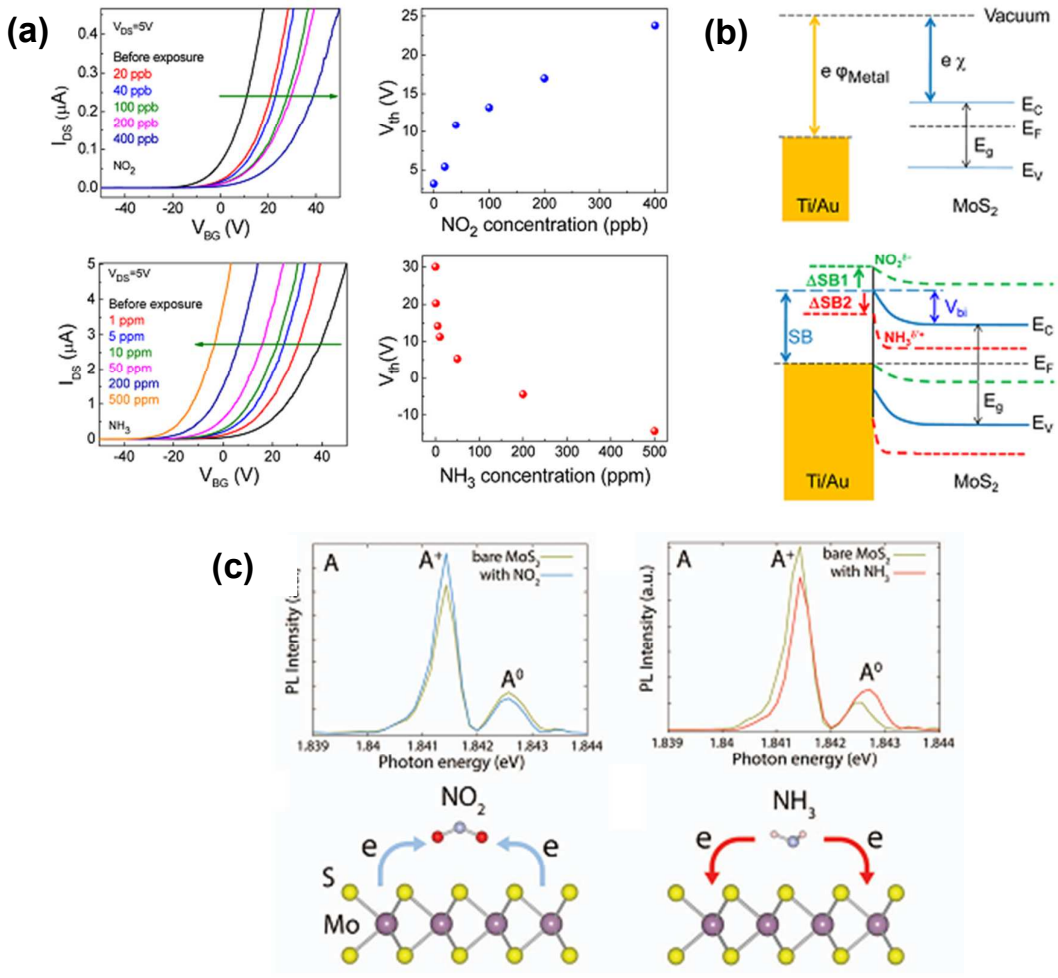

Fig. 3 (a) Transfer characteristics of an MoS_2 FETs upon exposure to NO_2 and NH_3 at different concentrations. Threshold voltage (V_{th}) versus gas concentrations for NO_2 and NH_3. (b) Proposed band alignment diagrams at the MoS_2-metal junctions (taken from[75]). (c) *In situ* PL spectra recorded from the MoS_2 with NO_2 and NH_3 molecules. Schematics of the charge density differences for MoS_2 in the presence of NO_2 and NH_3 gas molecules. NO_2 molecules on the surface of MoS_2 act as electron acceptors, whereas NH_3 molecules act as electron donors, from ref[76].

atomically thin layers[85,86]. Other layered metal chalcogenides like WS_2 and SnS_2 have also been studied for gas sensor application[87,88]. To date only conductometric gas sensors have been fabricated for the detection of vapours like triethylamine, ammonia, NO using MoS_2 devices. Compared to CNT based gas sensor, single layer MoS_2 exhibits higher sensitivity and selectivity towards volatile organic compounds (VOCs) at room temperature over a concentration range from 50 to 5000 ppm[89]. He *et al.* studied the NO_2 gas sensing properties of flexible thin film transistor (TFT) arrays based on MoS_2. For the fabrication of TFT, rGO patterned polyethylene terephthalate (PET) substrate was used as drain and source electrodes. A methanolic dispersion of MoS_2 was spin coated onto the PET substrate, which was used as a channel material. The sensor showed excellent sensing performance towards NO_2 compared to a similar device based on an rGO film. The sensing performance of platinum nanoparticle functionalized MoS_2 was also measured and found to have a sensitivity three times higher than for rGO, rGO-PtNPs and MoS_2[90]. In other work by Late and co-workers, the effect of layer thickness on the gas sensing performance of MoS_2 FET was studied. Using micromechanical exfoliation, two and five layer samples were prepared and used to detect gases such as NO_2, NH_3 and water vapour. A schematic and photograph of the MoS_2 transistor based sensor is shown in Fig. 4a-b. It was observed that unlike the two layer device, the five layer sample had a stable response with excellent sensitivity and recovery. Optical and SEM images of the two layer and five layer MoS_2 device, along with the sensor response and calibration data are displayed in Fig. 4c-h. Another interesting observation from this work is that the application of positive and negative gate bias influenced the gate resistance of the FET device, making MoS_2 more selective to NH_3 and NO_2 gases[91]. Very recently, Kim *et al.* developed a tunable and highly selective VOC sensor for analysis of lung cancer, based on a mercaptoundecanoic acid functionalized MoS_2 where the conjugated ligand influenced the sensor responses towards different VOC's [92]. In addition to MoS_2, BN

nanosheets are emerging as novel materials for gas sensors. Several reports describing computational and modelling studies of BN by DFT and Ab-initio methods revealed that BN nanosheets have a high adsorbing capacity for gas molecules and can be expected to exhibit high performance as gas sensors[93–98]. In a recent study, the methane sensing properties of BN nanosheets was demonstrated. The sensor had a systematic response in the presence and absence of analyte gas molecules[99]. Table 1 summarises gas sensors based on various 2D layered inorganic materials.

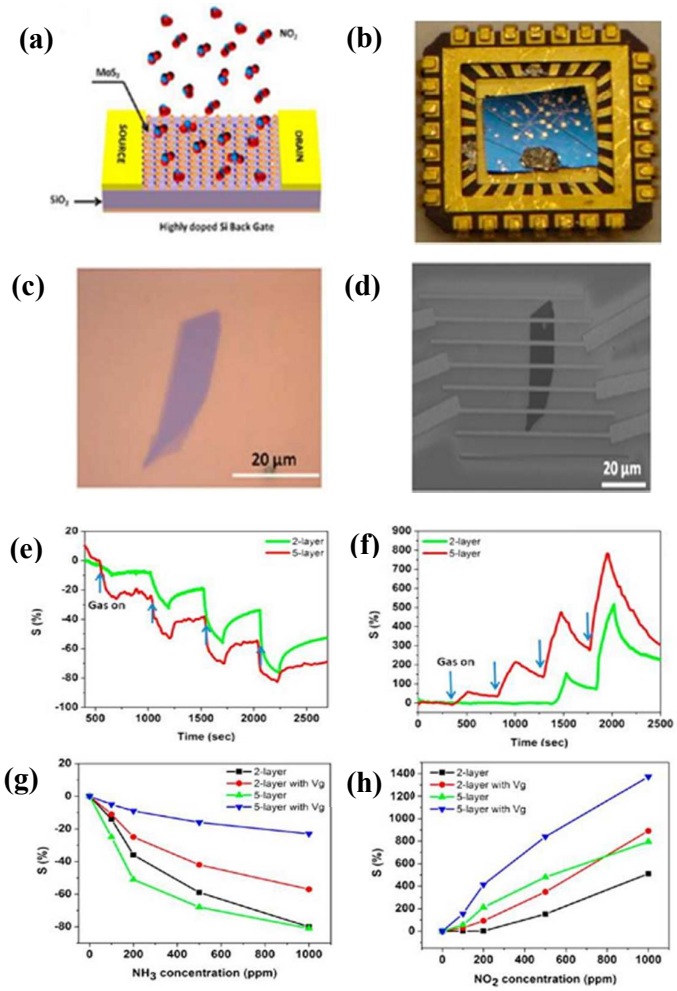

Fig. 4 (a) Schematic of the MoS_2 transistor-based NO_2 gas-sensing device. (b) Optical photograph of the MoS_2 sensing device mounted on the chip. (c) Optical image of two-layer MoS_2 sheet. (d) SEM image of two-layer MoS_2 transistor device. Comparison of two- and five-layer MoS_2 sensor performance with (e) NH_3 and (f) NO_2 (for 100, 200, 500, 1000 ppm). Sensitivity as a function of concentration (in ppm) for two-layer and five-layer MoS_2 sheets for (g) NH_3 and (H) NO_2. Data from ref. 132.

Table 1 Summary of gas sensors based on various 2D layered inorganic materials

S. No	Material	Detected gases or vapours	Sensor type	References
1	MoS_2 monolayer	Triethylamine	Conductometric	89
2	MoS_2 and MoS_2 -Pt	NO_2	TFT	90
3	Two and five layer MoS_2	Ammonia and NO_2	FET	91
4	Mercaptoundecanoic acid conjugated MoS_2	Toluene, hexane, Ethanol, propanol and acetone	Chemiresistor	92
5	Single and Multilayer MoS_2	NO	FET	90
6	MoS_2 nanosheets	Humidity	Chemiresistor	62
7	MoS_2 nanosheets	Ammonia	FET	16
8	MoS_2 nanosheets	Triethylamine	Conductometric	87
9	Monolayer MoS_2	Ammonia and NO_2	Schottky device	100
10	MoS_2- PANI	Hg vapour	Chemiresistor	101
11	SnS_2 nanoflakes	Nitroaniline	I-V	102
12	Flower-shaped SnS_2	Ammonia	Chemiresistor	88
13	h-BN nanosheets	Methane	Conductometric	99
14	VS_2	Humidity	Chemiresistor	103

3.2 Electrochemical Sensors

3.2.1 Mechanism involved in electrochemical sensing

Electrochemical sensors have been used for decades for the detection of various chemical species due to simplicity, low cost, high sensitivity and selectivity. The use of nanostructured materials as a recognition layer in electrochemical sensors has been widely reported because of many advantages including enhanced mass transport, high surface area, high sensitivity and improved signal to noise ratio[104,105]. Many materials have been studied, including metal nanoparticles, nanostructured metal oxides, nano conducting polymers, carbon nanotubes, graphene and nanocomposites consisting of either metal - metal oxides, mixed metal oxides, conducting polymers with metals or metal oxides, CNTs and graphene with metals or metal oxides or conducting polymers[106–120]. Recently, 2D-LIN based materials like MoS_2, WS_2, SnS_2, FeS_2 and Ni_3S_2 have been used as sensing materials for electrochemical sensors because of their high electrical conductivity, superior electrochemical properties due to edge effects, and enhanced surface to volume ratio compared to traditional metal oxides and conducting polymers. Nanocomposites of MoS_2, WS_2 and SnS_2 and Ni_3S_2 with graphene and CNT have been used as active materials to improve the performance of electrochemical sensors[121–124]. In addition, noble metals such as Au have also been incorporated along with these materials to enhance the sensor signals[125–127].

The working principle of an electrochemical sensor is mainly based on electron transfer between the surface of a working electrode (recognition layer) and target analyte (i.e. electrode-electrolyte interface) suspended in an appropriate electrolyte solution. A typical electrochemical sensor consists of a working, counter and reference electrode respectively. Normally, three techniques are used for the detection of electroactive species *viz.* cyclic

voltammetry, amperometry and potentiometry. Cyclic voltammetry is one of the most useful and versatile technique used for deriving information about the mechanism of the electrochemical reactions

Recently, Huang *et al.* fabricated an electrochemical sensor for the detection of bis-phenol using MoS_2 nanoflowers-Chitosan-Au nanoparticle modified glassy carbon electrode (GCE) [128]. The cyclic voltammetry data is reproduced in Fig. 5a showing that the MoS_2/Chitosan-Au modified GCE has a sharp anodic peak with enhanced current at about 0.9 V in the presence of bisphenol with no reduction peak. Thus it was inferred that the bisphenol molecules undergo irreversible oxidation this potential. From scan rate studies, the number of electrons transferred during the oxidation reaction was calculated as 2. The mechanism is shown in Fig. 5b. In another study, the electrochemical sensing of tryptophan was measured using nanocomposites of Ag-decorated MoS_2 nanosheets with chitosan[129]. During anodic scan, tryptophan undergoes an irreversible oxidation reaction (Fig. 5c) with a two electron transfer process; the mechanism is shown in Fig. 5d.

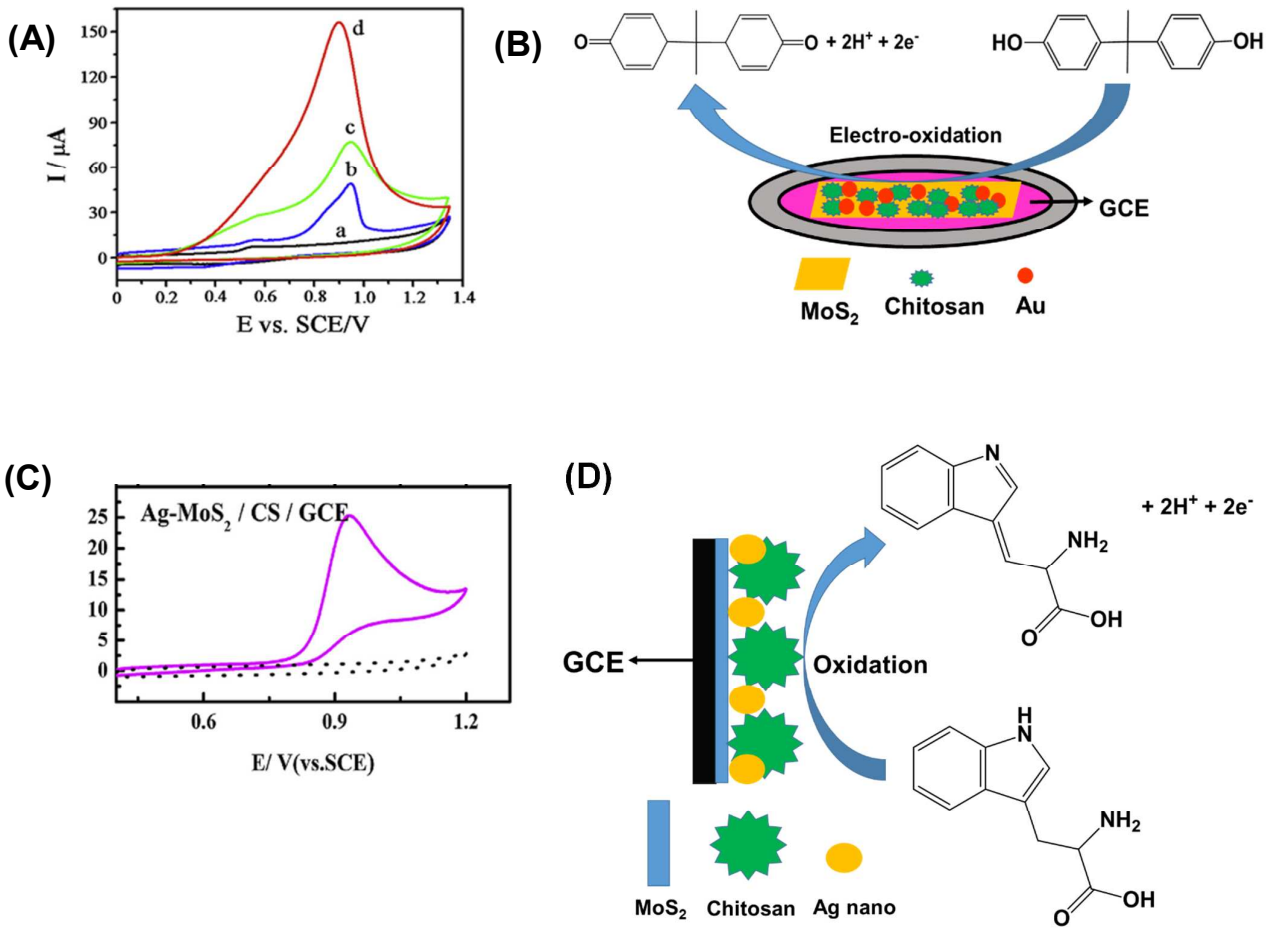

Fig. 5 (A) Cyclic voltammograms of (a) bare GCE (b) AuNPs/GCE, (c) MoS_2/GCE and (d) AuNPs/MoS_2/GCE in 0.1 M PBS (pH 7.0) containing 50 μM bisphenol. Scan rate: 100 mV s^{-1} [128] (B) Possible schematic illustration of the bisphenol sensing mechanism at a AuNPs/MoS_2 modified GCE. (C) Cyclic voltammogram of Ag-MoS_2/CS/GCE in the absence (dash line) and presence (solid line) of 0.1 mM tryptophan in 0.1 M phosphate buffer solution. of 0.1 mM tryptophan in 0.1 M phosphate buffer solution (pH 6.0).[129] (D) possible schematic diagram of tryptophan oxidation mechanism at Ag-MoS_2/CS/GCE.

3.2.2 Current status

Many reports have appeared in the literature on the use of layered inorganic nanomaterials for electrochemical sensors. Some of the 2D-LINs like MoS_2, WS_2 and SnS_2 have been investigated as electrochemical sensors. Recently, Chakraborty *et al.* made a comparativestudy of the H_2O_2 sensing properties of cathodically and anodically deposited FeS_2 thin films on ITO substrates where the sensing property was found to depend on the morphology of the samples. The cathodically deposited film showed a compact layered structure and exhibited poor electrocatalytic activity, while the macroporous anodic films showed good catalytic activity towards H_2O_2. The sensor had a sensitivity of 604.8 μAmM^{-1} in the linear range from 10 μM to 1.9 mM, with a detection limit value of 4 μM[66]. Metal chalcogenides have potential applications in many fields such as catalysts, supercapacitors, lubricants and so on. However, there are few reports concerning applications for electrochemical sensor. This is because 2D-LINs like MoS_2 or WS_2 have very low conductivity, which makes them unsuitable as electrode materials for sensors. In order to overcome this difficulty, hybridization of metal chalcogenides with other conducting materials like nanostructured metals, nanostructured conducting polymers, carbon nanotubes and graphene has been attempted, and these hybrid materials expect to show synergetic effects in sensor applications. Li and co-workers[63,130] developed a glucose sensor based on Ni and Cu nanoparticle functionalized MoS_2 nanosheets. Their results showed that Ni exhibited a higher sensitivity than Cu. A sensitivity of 1824 $\mu A\ mM^{-1}\ cm^{-2}$ was obtained for Ni nanoparticles with Cu nanoparticles at 1055 $\mu A\ mM^{-1}\ cm^{-2}$ over a linear range from 0-4mM.

Au nanoparticle decorated MoS_2 nanosheets have been used for the simultaneous detection of dopamine, uric acid and ascorbic acid[125,126]. Fig. 6a-c shows a schematic illustration of a MoS_2 nanosheet based electrochemical sensors, and SEM images of MoS_2 nanosheets. Fig. 6d shows the cyclic voltammograms of gold decorated MoS_2 nanosheets measured in 0.1 M phosphate buffer solution solution (pH 7.0) containing 20 mM ascorbic acid, 1mM dopamine and 10 mM uric acid Polyaniline is one of the most widely used conducting polymers with applications in gas sensing[131], batteries[132], supercapacitors[133] and corrosion protection[134]. It is low cost, easy to prepare, has excellent environmental and chemical stability and remarkable electrical properties which can be easily controlled by protonation and deprotonation. These properties make polyaniline a promising material for electrochemical sensors. Recently, Huang *et al*. demonstrated electrochemical detection of dopamine using MoS_2-polyaniline-gold nanocomposites. The sensor exhibited good electrocatalytic activity towards oxidation of dopamine with a linear response range from 1 to 500 μM and a detection limit of 0.1 μM (S/N = 3). Likewise, the sensor showed good sensitivity for dopamine in human urine[135]. An electrochemical sensor has been fabricated for the detection of acetaminophen using MoS_2–graphene nanocomposites. Compared to bare MoS_2, electrodes composed of MoS_2-graphene showed superior performance which might be because the composite acts as an efficient electron promoting material, and the synergism between the layered MoS_2 and graphene enhances the electrocatalytic processes. The sensor exhibited excellent sensing performance, with a detection limit of 2.0×10^{-8} M (S/N = 3) and linear range from 0.1–100 μM[136]. Huang *et al.* studied the performance of layered WS_2-graphene nanocomposites for the simultaneous detection of catechol, resorcinol and hydroquinone. Compared to bare GCE and graphene modified electrodes, WS_2-graphene showed enhanced electrocatalytic behaviour towards the oxidation of catechol, resorcinol and hydroquinone[122]. Recently, chitosan based nanocomposites have been widely employed as an electrochemical sensor

because of its ability to form uniform films on an electrode surface with high permeability and good adhesion. Also, it is bio-compatible and possess good electron transfer properties after swelling in a reaction mixture. It has large numbers of amino groups which are favourable sites for enzyme or metal immobilization. Xia *et al.* fabricated an electrochemical sensor for the detection of tryptophan using Ag functionalized MoS_2-chitosan nanocomposites. Fig.6 e-f shows the DPV and calibration plot, along with the interference data measured for Au functionalized MoS_2-chitosan nanocomposites for different concentrations of tryptophan. The novel composite exhibited good sensing performance towards tryptophan, and electrochemical kinetic parameters like transferred electron number, electron transfer coefficient, and surface coverage for the oxidation of tryptophan were determined from the results[129]. Table 2 shows a compilation of the sensor parameters for various 2D metal chalcogenide nanocomposites based electrochemical sensors.

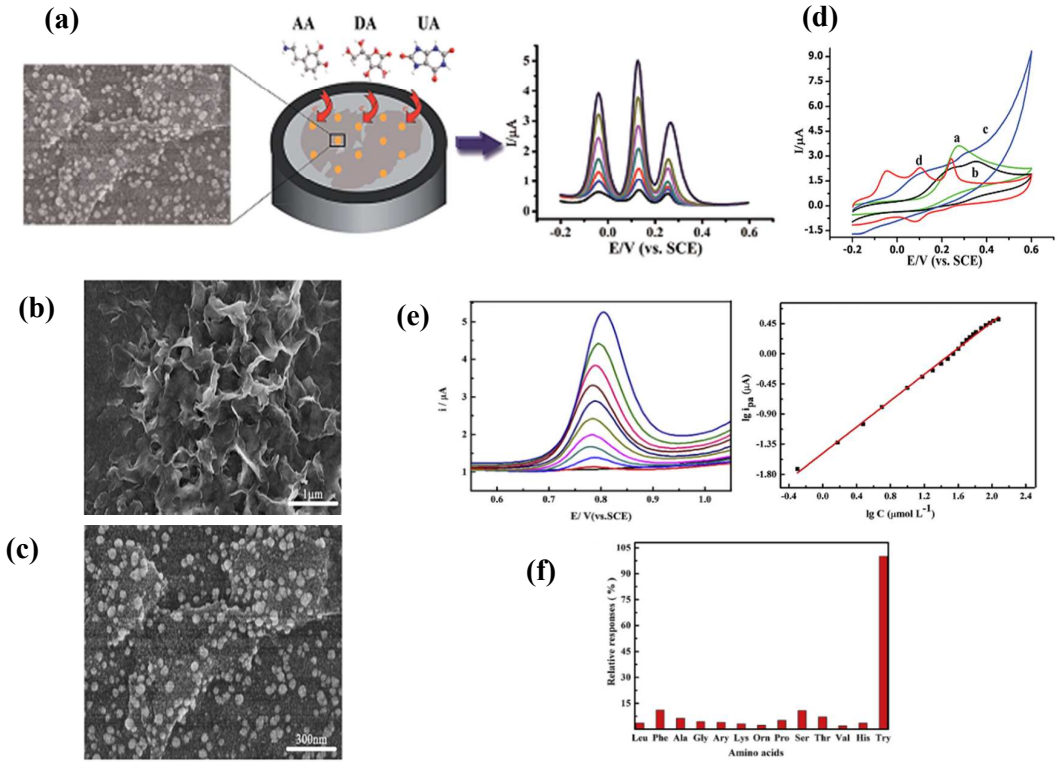

Fig. 6 (a) Schematic illustration of MoS_2-based electrochemical sensors. SEM images of the (b) MoS_2 and (c) AuNPs@MoS_2 nanostructures on ITO. (d) Cyclic voltammograms of (a) bare GCE and (b) AuNPs/GCE (c) MoS_2/GCE (d) AuNPs@MoS_2/GCE in 0.1 M PB solution (pH 7.0) containing of 20 mM AA, 1mM DA and 10 mM UA. Scan rate: 100 mV s^{-1}. Ref.[125] (e) DPVs obtained at Ag-MoS_2/CS/GCE in 0.1 M phosphate buffer solution (pH 6.0) containing low concentrations of tryptophan along with the calibration plot (f) The electrochemical responses for tryptophan and other amino acids (with the concentration 50-fold) on the Ag-MoS_2/CS/GCE. Taking the response of tryptophan as 100%. Ref.[129]

Table 2 Compilation of the sensor parameters of various 2D metal chalcogenides nanocomposites based electrochemical sensors.

S. No	Material	Analyte detected	Sensitivity	Linear range	Low detection limit	Ref.
1	MoS_2-Ni nanoparticles	Glucose	1824 μA mM^{-1}	0- 4 mM	0.31 μM	63
2	MoS_2-Cu nanoparticles	Glucose	1055 μA mM^{-1}	0- 4 mM	-	130
3	Au-decorated MoS_2	AA, DA and UA	-	AA - 10^{-3} - 7×10^{4} μM DA - 0.05 - 4×10^{3} μM UA - 10 - 7×10^{3} μM	AA - 100 μM DA - 0.05 μM UA - 10 μM	126
4	Au-decorated MoS_2	Dopamine	-	0.1 to 200 μM	80 nM	125
5	MoS_2-PANI-Au	Dopamine	-	1-500 μM	0.1 μM	135
6	MoS_2–graphene	Acetaminophen	-	0.1 – 100 μM	0.02 μM	136
7	WS_2–graphene	CA, RS and HQ	-	CA- 1 - 100 μ mol dm^{-3} RS - 1 - 100 μ mol dm^{-3} HQ -1 - 100 μ mol dm^{-3}	CA - 0.2 μ mol dm^{-3} RS - 0.1 μ mol dm^{-3} HQ - 0.1 μ mol dm^{-3}	122
8	MoS_2-Chitosan-Ag	Tryptophan	-	0.5- 120 mM	0.05 μM	129
9	FeS_2	H_2O_2	604.8 μA mM^{-1}	10 μM - 1.9 mM	4 μM	66
10	MoS_2-Chitosan-Au	Bisphenol-A	-	0.05-100 μM	0.005 μM	128
11	Poly(diallyldimethylammonium chloride) - graphene-MoS_2	Eugenol	-	0.1–440 μM	0.036 μ mol L^{-1}	137

3.3 Electrochemical and FET based biosensors

3.3.1 Possible mechanisms

The working principle of these biosensors is similar to that of electrochemical sensors, except for the recognition layer where a bio-material is immobilized and used as a transducer. Biological materials such as enzymes, antibodies, nucleic acids, hormones and tissues are used as a bio-recognition elements[138]. During the measurement, analyte molecules interact with the sensing layer giving rise to an electrical signal. The performance of an electrochemical biosensor depends on the chemical and physical conditions of the experiment such as pH, temperature, contaminants and thickness, and stability of the active material. Among the various 2D-LIN materials, MoS_2 and SnS_2 have been extensively employed as electrochemical biosensors.

Very recently, a sensor for hydrogen peroxide (H_2O_2) has been developed by fabricating an electrochemical sensor with horseradish peroxidase (HRP) immobilized MoS_2-graphene as a working electrode[139]. When H_2O_2 was added to the hydroquinone electrolyte solution, the immobilized HRP was oxidized during anodic scan, simultaneously oxidizing the hydroquinone. As a result, benzoquinone was formed as a reaction product which was subsequently reduced producing the electrical response. These catalytic processes are expressed by the following equations. The sensing mechanism is illustrated in Fig. 7a

$$\mathrm{HRP} + \mathrm{H_2O_2} \rightarrow \mathrm{HRP(Ox)} + \mathrm{H_2O} \quad (2)$$

$$\mathrm{HRP} + \mathrm{hydroquinone} \rightarrow \mathrm{HRP(red)} + \mathrm{benzoquinone} \quad (3)$$

$$\mathrm{Benzoquinone} + 2e^- + 2\mathrm{H^+} \rightarrow \mathrm{hydroquinone} \quad (4)$$

Field effect transistor (FET) biosensors are being developed to detect various biological species such as DNA, cells and proteins. These devices offer desirable advantages such as high sensitivity, low detection limit, label free detection, low power consumption,

portability, large scale production and the possibility of integrating both sensor and measurement system in a single chip. In a conventional FET device, current flow through the channel between source and drain is controlled by gate electrode which is coupled capacitively via a dielectric to the channel. An FET biosensors, has a dielectric material that is functionalized with a receptor molecules. When the device is exposed to a target analyte, the receptor molecules selectively bind the biomolecules, modulating the channel conductance, which is then transduced into an electrical output signal. Current and emerging challenges of FET based biosensing has been reviewed recently[140]. Fig 7b shows a schematic diagram of a typical MoS_2 based FET biosensor.

Recently, Sarkar *et al.* demonstrated detection of the protein streptavidin using an MoS_2 FET biosensor in which the dielectric layer was functionalised with biotin[24] giving a large change in source-drain current. When protein-free buffer was added, the device current remained unchanged. Fig. 7c and d shows a schematic of the sensing mechanism

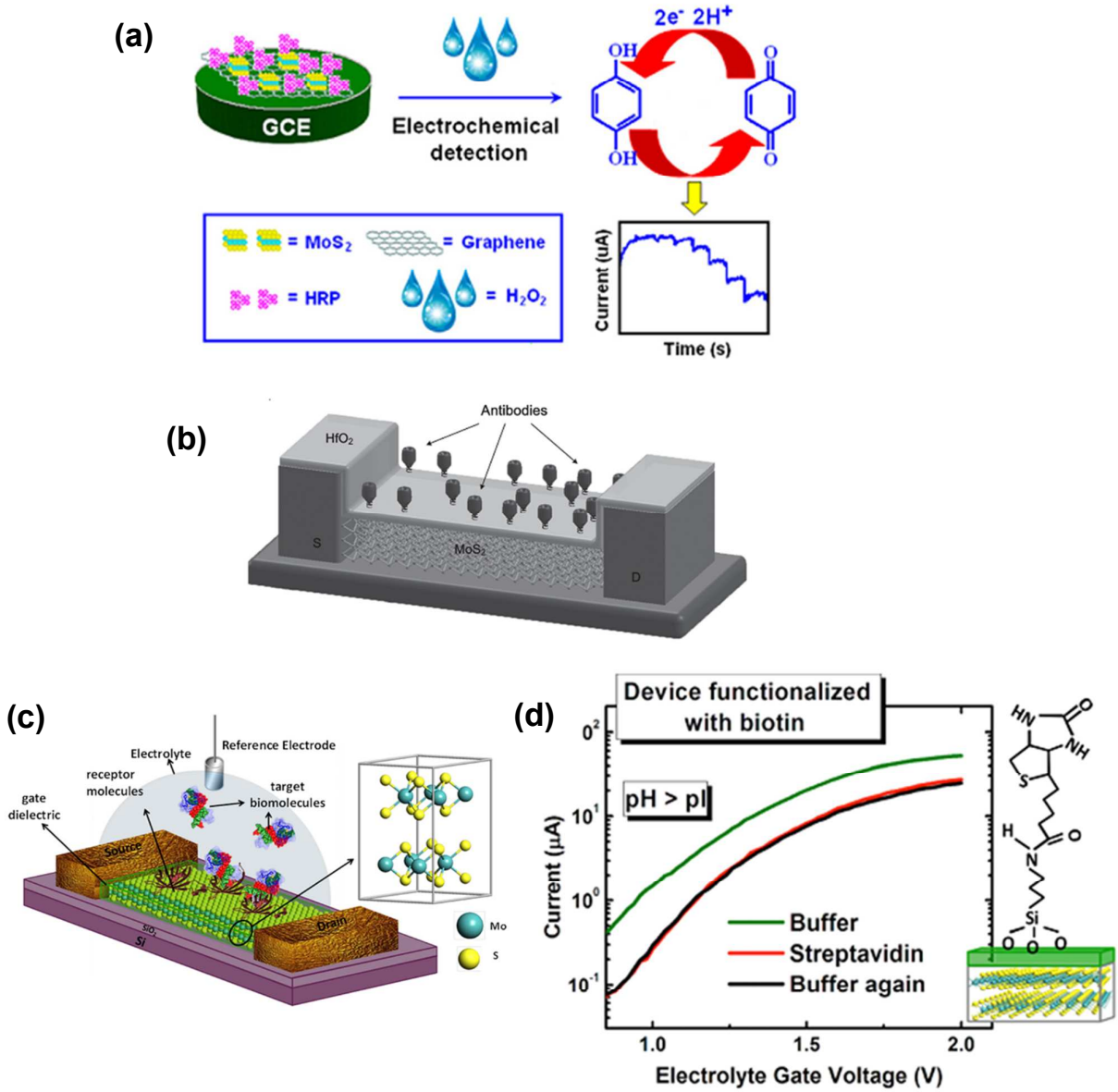

Fig. 7 (a) Schematic of H_2O_2 sensing by a HRP–MoS_2–Gr electrochemical biosensor.[139] (b) Diagrammatic representation of an MoS_2 FET biosensor. (c) & (d) Diagram of MoS_2-based FET biosensor and its response to streptavidin[24].

3.3.2 Current status

Compared to conventional lab-based analytical techniques, biosensor offers high sensitivity and specificity, enabling real time analysis in complex mixtures, simple fabrication and operation without the need for expensive instrumentation and cost effectiveness. Many different kinds of materials based on 2D LINs like MoS_2, SnS_2 and $BiSe_2$ have been used to fabricate electrochemical biosensors, but there are few reports on the use of simple MoS_2 films for electrochemical biosensors. Wu *et al.* was able to sense small molecules like glucose, dopamine, uric acid and ascorbic acid using GOD immobilized on monolayers of MoS_2 prepared by the electrochemical reduction of a self-assembled MoS_2 bulk layer. The sensor had a good response to glucose and high selectivity towards dopamine in the presence of ascorbic acid and dopamine[121]. Enzymatic detection of glucose and non-enzymatic detection of dopamine and ascorbic acid were also demonstrated out using ultrathin MoS_2 nanosheets[141]. It was observed that the sensor exhibited maximum response to dopamine, attributed to the electrostatic attraction between positively charged dopamine and negatively charged MoS_2. The negatively charged ascorbic acid molecules were electrostatically repelled. Another glucose biosensor was demonstrated using co-electrodeposited Prussian Blue/Bi_2Se_3 nanocomposites in which GOD and chitosan were immobilized on an electrode surface. The insulating nature of selenide helped in forming smaller particles of Prussian Blue with better pH stability. The sensor exhibited a sensitivity of 24.55 $\mu A\ mM^{-1}\ cm^{-2}$ with a good linear range from 0.01–11.02 mM[142]. As discussed in section 4.2, bare metal chalcogenides have very low conductivity and are not suitable for use as electrode materials in electrochemical biosensors. Therefore, hybridization of layered inorganic materials with metal nanoparticles, carbon nanotubes and graphene is essential to overcome this problem. The majority of the electrochemical biosensor so far reported are based on MX_2-graphene nanocomposites. MoS_2 and MoS_2-graphene electrodes modified with

the enzyme horseradish peroxidase were used for electrochemical biosensing of hydrogen peroxide[139,143]. Recently, Huang *et al.* reported the use of WS_2-graphene nanocomposites with gold nanoparticles for electrochemical DNA sensing. A schematic of the Au/MoS_2/MWCNT biosensor is shown in Fig. 8A. Fig. 8B shows TEM images of the MoS_2 nanosheets and MoS_2/MWCNT composites. The sensor exhibited a good relationship between the measured current and target DNA concentration over the range 0.01 to 500 pM, with a detection limit of 0.0023 pM. The DNA biosensor also showed good discrimination between a single base mismatch, three-base mismatch and non-complementary DNA[144]. The CV data of the nanocomposite modified electrodes for different sequences of DNA is shown in Fig. 8C. Like MoS_2 and WS_2, nanocomposites of SnS_2 with gold and SWCNT have also been used to manufacture electrochemical biosensors for glucose, dopamine and uric acid[123,145,146]. The response of GOx/MWCNTs–SnS_2/Nafion modified GCE in different concentrations of glucose is shown in Fig. 8D. A list of electrochemical biosensors based on various 2D layered inorganic materials is shown in Table 3.

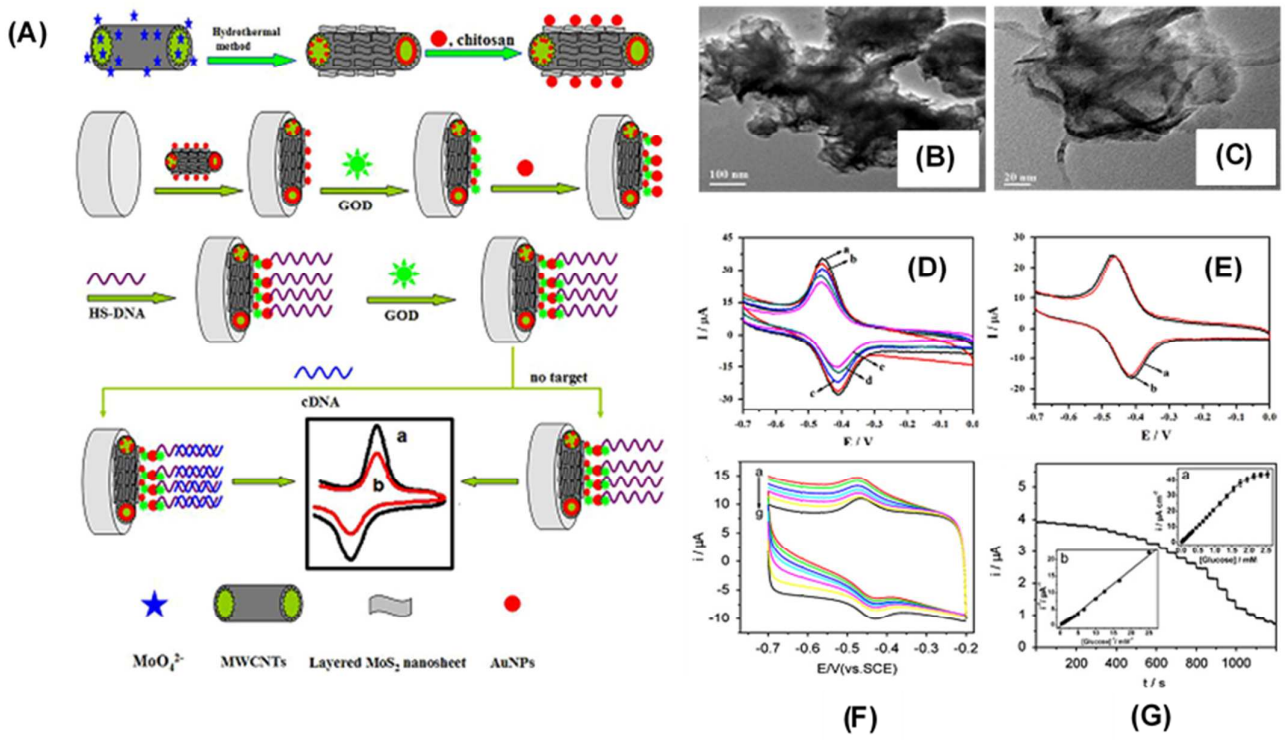

Fig. 8 (A) Schematic diagram of an electrochemical DNA biosensor (B and C) TEM images of MoS_2 nanosheets and MoS_2/MWCNT composites. (D) CVs of (a) GOD/S1/AuNP/GOD/AuNP/MoS_2/MWCNT/GCE and its hybridization with 1.0×10^{-11} mol L^{-1} different S2 sequence 0.1 M PBS (6.0) containing 0.9% NaCl. (b) noncomplementary sequence (c) three-based mismatch sequence (d) single-based mismatch sequence and (e) complementary sequence (E) first cycle and fifth cycles of CV measurements of GOD/S1/AuNP/ MoS_2/MWCNT modified GCE in 0.1 M PBS (pH 6.0) containing 0.9% NaCl after hybridization with complementary ss DNA sequence. Ref.[144] (F) CVs of the GOx/MWCNTs–SnS_2/Nafion modified GCE in 0.1 M air-saturated and N2 saturated phosphate buffer solution (pH 6.0) containing different concentrations of glucose at a scan rate of 50 mV s^{-1}; (G) Typical steady-state response of the GOx/MWCNTs–SnS_2/Nafion/GCE on successive addition of glucose into 0.1 M air-saturated phosphate buffer solution (pH 6.0) at an applied potential of -0.43 V. Inset at top calibration curve of the GOx/MWCNTs–SnS_2/Nafion/GCE for glucose; at bottom : plot of j^{-1} vs. $[Glucose]^{-1}$. Ref.[123]

Table 3 List of electrochemical biosensors based on various 2D layered inorganic materials

S. No	Material	Analyte detected	Sensitivity	Linear range	Low detection limit	Ref.
1	APTES/chitosan/rMoS_2/GOD	Glucose	-	0 – 20 mM	-	121
2	GOx/MoS_2	Glucose	-	-	-	141
3	PB/Bi_2Se_3/GOx	Glucose	24.55 μA mM^{-1} cm^{-2}	1.0×10^{-5} –1.1×10^{-2} M	3.8 μM	142
4	HRP/MoS_2	H_2O_2	-	1.0×10^{-6} - 9.5×10^{-4} M	2.6×10^{-7} M	143
5	HRP/MoS_2/Gr	H_2O_2	679.7 μA mM^{-1} cm^{-2}	0.2 μM–1.103 mM	0.049 μM	139
6	WS_2/Gr	DNA	-	0.00001–0.5 nM	0.0023 pM	147
7	GOx/Au/SnS_2/chitosan	Glucose	21.78 mA M^{-1} cm^{-2}	0.02-1.32 mM	0.001 mM	127
8	GOx/MWCNTs–SnS_2	Glucose	-	0.02–1.95 nM	0.004 nM	123
9	SWCNT/CS–SnS_2	AA, DA and UA	-	-	-	146
10	Nafion-GOx/Au/MoS_2	Glucose	-	10–300 μM	2.8 μM	145
11	GOD/Au/MoS_2/MWCNTs	DNA	-	0.001–100 nM	0.11 pM	144
12	Nafion/Hb/MoS_2	H_2O_2	21.65 mA M^{-1} cm^{-2}	20–180 μmol L^{-1}	6.7 μmol L^{-1}	148
13	MoS_2	Protein molecules	-	-	-	24

3.4 2D-LIN based SERS sensors

3.4.1 SERS sensing mechanism

SERS is a non-destructive technique mainly used for the detection of chemical and biological species, whereby, the intensity of weak Raman signals can be magnified by several orders of magnitude. The enhancement of a SERS signal depends on the nature and shape of the nanostructured materials, porosity, orientation and the substrate onto which the nanomaterial is deposited. An excellent review article on the concepts and chemical applications of SERS can be found in[149]. The detection of chemical and biological species by a SERS sensor is based on the enhancement of a Raman signal upon the adsorption of a sensing species. Two major mechanisms are responsible for the enhancement of Raman signals (for reviews see refs[150–153]), namely electromagnetic and charge transfer. For these two mechanisms to occur, a species must be adsorbed on an appropriately nano-patterned metal substrate. Different Raman enhancement mechanisms have been proposed for different 2D materials; these vary from material to material depending on its atomic orientation and the properties of the atomic species involved. For example, strong dipole−dipole coupling may occur for h-BN, and both charge transfer and dipole−dipole coupling may occur, although weaker in magnitude, for MoS_2[154].

Electromagnetic mechanism: When a monochromatic light source like a laser is incident on a nanostructured metal substrate, the incident light excites surface plasmons. For a nanostructured metal surface with high roughness, the plasmons create a local electromagnetic field which amplifies the Raman scattering from an adsorbed analyte molecule. In order to excite electrons on the metal surface, the wavelength of the incident light must be comparable with the wavelength of the plasmons created. Normally, monochromatic light with wavelength value between 450 and 1064 nm can be used, and to

match these wavelengths, metals like copper, silver and gold are used as substrates in SERS sensors[155–157].

Charge-transfer (CT) mechanism: In SERS sensors, CT processes occur between the adsorbed analyte molecules and the metal surface. When light is incident on a metal surface, electrons get excited forming electron-hole pairs. From this pair, energy is transferred to analyte molecules through new metal bonds. Raman process occur in the analyte molecules and the energy is transferred to the metal surface. Thus the Raman signals are enhanced due to this chemical processes. In other words, the wavelength of the excited light is resonant with the charge transfer electronic states between the metal and adsorbed molecules.

3.4.2 Current status

SERS based chemical sensors have attracted widespread attention because they offer advantages such as high specificity and very low limits of detection. A plethora of materials like gold and silver nanoparticles, titanium oxide, zinc oxide, silicon dioxide and carbon nanotubes have been used in SERS. After the discovery of graphene, the generation of SERS on 2D surfaces is attracting interest. 2D layered materials with flat surfaces are promising materials for SERS sensors. These 2D materials have no dangling bonds and the absorbed analyte molecules sit on the surface in face–on configuration. These materials are expected to show different Raman enhancement factors compared to conventional nanostructured materials. In a recent study by Perkins *et al.* the chemical sensing properties of MoS_2 for trimethylamine was measured; the sensor exhibited high selectivity towards a wide range of analytes attributed to the charge redistribution induced by the perturbations on the MoS_2 surface[89]. It was established that surface modification leads to a strong interaction between MoS_2 and the analyte molecules. Using this approach, several reports have appeared describing the detection of chemical species by SERS using 2D layered metal chalcogenides.

Very recently, a comparison of SERS sensing of rhodamine dye with oxygen and argon treated MoS_2 was studied, and the results compared with a pristine surface. Fig. 9a shows optical and AFM images of MoS_2 nanoflakes on a SiO_2 /Si substrate. Compared to the pristine MoS_2, plasma (argon and oxygen) treated MoS_2 exhibited enhanced Raman signals. This observation is explained by the fact that plasma bombardment of the MoS_2 surface created structural disorders which in turn led to the formation of local dipoles and as a result, the Raman signals was enhanced due to the change of symmetry[158]. Fig. 9b-d shows Raman spectra of different layers of bare and R6G molecules adsorbed onto MoS_2 nanoflakes. In another study, SERS detection of 2-mercaptobenzimidazole using MoS_2-silver nanocomposite was reported. The nanocomposite exhibited high SERS activity, attributed to the large electromagnetic fields caused by the aggregation of silver nanoparticles on MoS_2 nanosheets[159].

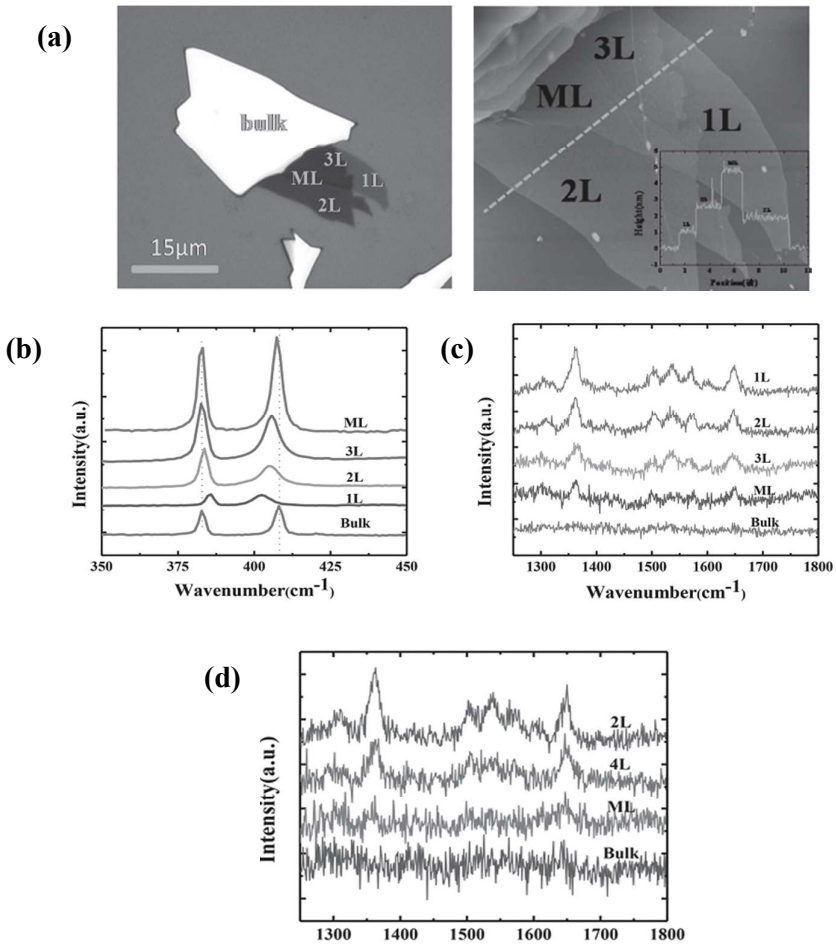

Fig. 9 (A) Optical image and AFM image of a typical MoS_2 nanoflake deposited on SiO_2 /Si. (B) Raman spectra of OT-MoS_2 nanoflake, including 1L, 2L, 3L, ML and bulk. (C) Raman spectra of R6G molecules on OT-MoS_2 samples with different thickness. (D) Raman spectra of R6G on suspended OT-MoS_2 nanoflakes with different thickness. Ref.[158].

3.5 2D-LIN based Photodetectors

3.5.1 Photodetection Mechanism

A photodetector is a light sensor that can transduce incident radiation into an electrical signal. Photodetectors have many applications such as space communication and detection of chemical and biological species. Fig. 10a shows a schematic illustration of a Sb_2Se_3 single nanowire based photodetector. The working mechanism of a photodetector is well-known and many reviews explain the details[160–162]. When light is incident on a semiconducting surface, electrons are excited and move to an energetic conductive state, leaving a hole. Fig. 10 b is the energy band diagram showing the density of states in atomically thin MoS_2 and depicting the formation of an electron-hole pair upon photon excitation. Thus, an electron-hole pair called excitons are formed as a result of photon excitation. When an electric field is applied, the electrons and holes drift inside the crystal lattice, constituting an electric current- the photocurrent. Fig. 10 c and d shows the response of Sb_2Se_3 photodetector in the dark and under illumination along with the time dependent photoresponse data.

The performance of the photodetector is characterized by various parameters such as sensitivity, external quantum efficiency, responsivity, detectivity and response and decay time. Sensitivity (S %) is defined as the ratio between the difference in photo current (I_{ph}) and dark current (I_{dark}) values to the dark current and is expressed as

$$S(\%) = \frac{I_{ph} - I_{dark}}{I_{dark}} \quad (5)$$

Another important parameter is the external quantum efficiency (η) which is defined as the number of electrons detected per number of incident photons and it can be represented as

$$\eta = \frac{hc\Delta I}{e\lambda PS} \quad (6)$$

where h is Planck's constant, c is velocity of light, ΔI is the photoexcited current, e is electron charge, λ is the excitation wavelength, P is the incident light power intensity and S is the effective area of photodetector. Responsivity (R) is the ratio of the number of incident photons per incident optical power, defined as

$$R = \frac{\eta \lambda q}{h\, c} \tag{7}$$

where λ is the wavelength of the incident photos and c the velocity of light. The ability of a photodetector to detect signal from noise is defined as detectivity (D):

$$D = \frac{I_{ph}}{\rho \sqrt{q I_{dark}}} \tag{8}$$

where ρ is the light intensity. In addition two parameters that determine the capability of a photodetector in practice are response time and recovery time. Response time is defined as the time taken for a photodetector to reach 90% of the maximum photocurrent value from its dark current value. Similarly, decay time is defined as the time taken by a photodetector to reach 10% of maximum photocurrent response.

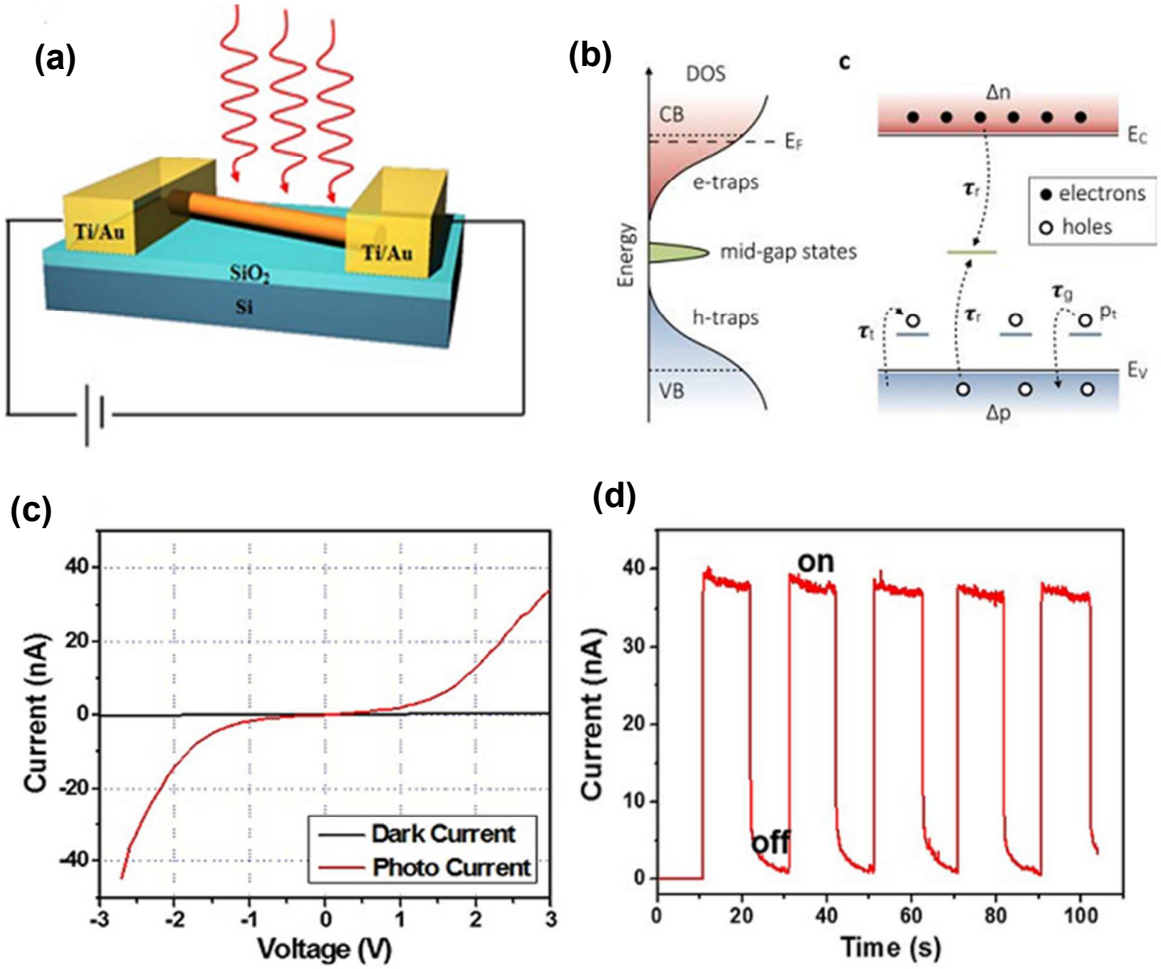

Fig. 10 (a) Schematic view of a Sb_2Se_3 single nanowire photodetector.[163] (b) Schematic drawing of the density-of-states in atomically thin MoS_2 (c) I-V plot of Sb_2Se_3 device in dark and under illumination condition (d) Time dependent current response of a photodetector[163].

3.5.2 Current status

Nanomaterial based photodetectors show improved light sensitivity compared to bulk counterparts, and have enhanced photocarrier life time due to their large surface to volume

ratio. Over the last seven years, graphene has been used for photodetectors because of its high carrier mobility, wide band absorption and short carrier life time. However, it also has limitations such as low photoresponsivity and low detectivity with low external quantum efficiency, which could be due to its low light absorption coefficient and fast rate of photoinduced carrier recombination[164–166]. In order to overcome this deficiency, it is important to explore other kinds of 2D layered materials for photodetection. A high performance photodetector has been fabricated using nanostructures of GaSe, a few layers thick prepared by exfoliation onto a SiO_2/Si substrate. Fig. 11A-E shows a drawing of the GaSe photodetector and the corresponding I-V curves, photocurrent and linear dynamic range measured at different wavelengths. Compared to the photoresponse data of GO, G and single layer MoS_2, the GaSe device shows excellent quantum efficiency, with a value of 1367 % and a response time of 20 ms[167]. A dye-sensitized photo detector was fabricated using a single layer MoS_2 treated with rhodamine 6G organic dye molecules; fig. 11F shows a schematic diagram. Compared to pristine MoS_2, the dye sensitized film shows excellent performance with a maximum photoresponsivity of 1.17 AW^{-1} and a photodetectivity of 1.5 $\times 10^7$ Jones and a total effective quantum efficiency (EQE) of 280 % at 520 nm[168]. Recently, Roy *et al.* fabricated a highly sensitive gate-tunable photo detector based on MoS_2-graphene hybrids. The binary heterostructures showed enhanced photoconductivity with remarkable optoelectronic functionality. The responsivity of the device was found to be nearly 1×10^{10} AW^{-1} at 130 K and 5×10^8 AW^{-1} at room temperature[169]. The photoswitching properties of the dye sensitized MoS_2 measured under alternating dark and light illumination is shown in Fig. 11G. Very recently, the photoresponsivity of a TiS_3 nanoribbon based FET was reported in which the as-prepared TiS_3 exhibited *n*-type semiconducting behaviour with a mobility of 2.6 $cm^2V^{-1}s^{-1}$ and ON/OFF ratios up to 10^4. The device displayed a ultrahigh photoresponse

of up to 2910 A W^{-1} with fast switching time of about 4 ms and a cut-off frequency of 1000 Hz[170]. Table 4 lists various 2D layered inorganic materials used in photodetectors.

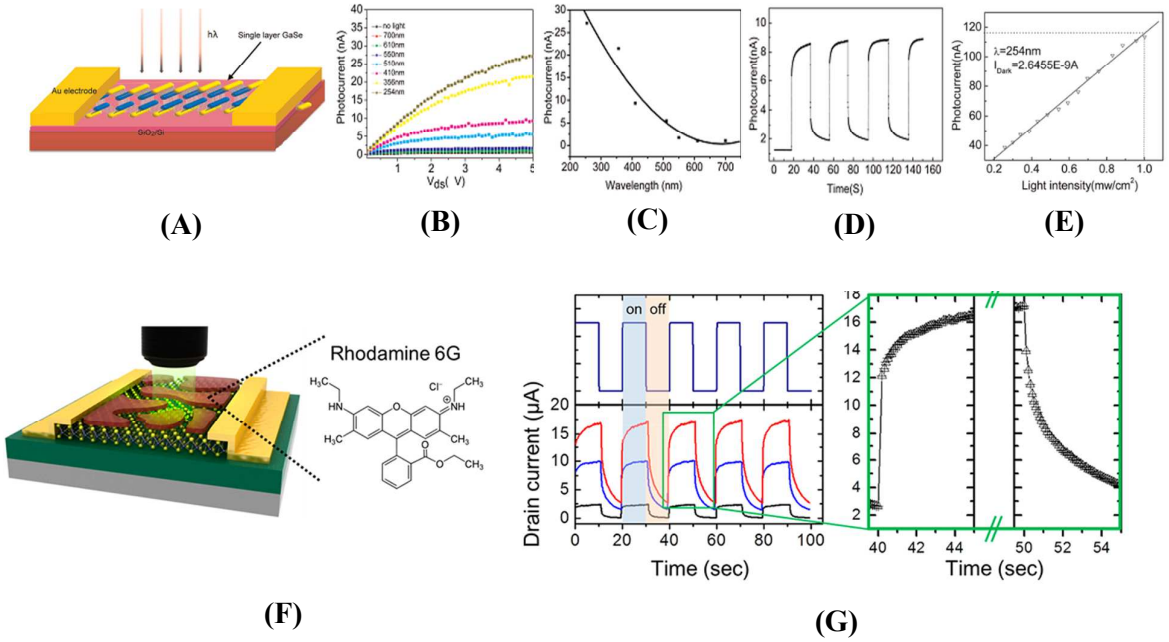

Fig. 11 (A) Schematic drawing of the GaSe photodetectors. (B) I-V curves of photodetectors illuminated with different wavelengths. (C) wavelength-dependent photocurrent; (D) photocurrent as function of time at a bias voltage of 1 V; (E) photocurrent as function of illumination density, linear dynamic range of the device under light irradiation of 254 nm.[167] (F) Schematic diagram of a single-layer MoS_2 photodetector treated with rhodamine 6G (R6G) organic dye molecules and chemical structure of the R6G dye. (G) Photoswitching characteristics of the R6G-sensitized MoS_2 photodetector at three different drain voltages (black = 1 V, blue = 3 V, and red = 5 V) under alternating dark and light illumination (λ= 520 nm and P= 1 mW)[168]

.

Table 4 List of various 2D layered inorganic materials used in photodetector applications.

S. No	Material	Photodetector parameters			References
		Response time	Maximum responsivity	External quantum efficiency	
1	Few-Layer GaSe Nanosheets	0.02 s	2.8 AW^{-1}	1367 %	167
2	GaSe Atomic Layers	-	17 mAW^{-1}	5.2	171
3	Single layer MoS_2	-	1.17 mAW^{-1}	280%	168
4	Graphene-MoS_2	~1 s	1×10^{10} AW^{-1} at 130 K 5×10^{8} AW^{-1} at RT	32 %	169
5	Few-Layer TiS_3 Nanoribbon	4 ms	2910 AW^{-1}		170
6	GaS Nanosheet on SiO_2/Si	<30 ms	4.2 AW^{-1}	2050 %	172
7	GaS Nanosheet on PET	<30 ms	19.2 AW^{-1}	9371 %	172
8	2D GaSe nanocrystals	-	2.8 AW^{-1}	-	173
9	Multilayer GaTe Flakes	6 ms,	10^4 AW^{-1}	-	174
10	Few-Layered InSe Photodetectors	~ 50 ms,	12 AW^{-1}	-	175
11	ZnS:Ga nanoribbons	~ 3.2 ms,	1.3×10^{19} cm $Hz^{1/2}W^{-1}$	-	176
12	MoO_3	-	56 AW^{-1}	10200 %	177

5 Future prospects

2D-LIN are attracting huge interest and are promising materials for sensor applications because of their layer-dependent physical and chemical properties. A variety of physical and chemical methods have been used to prepare 2D-LIN metal chalcogenides, either as powders or thin films. Among these methods, micromechanical exfoliation produces monolayers or a few layers of 2D materials with high purity and crystallinity. Other physical methods such as unzipping and PLD have also been used to produce thin layers of 2D materials. In chemical methods, hydrothermal and solvothermal methods have been used to make bulk powders. Liquid exfoliation is an easy technique that can produce large quantities of inorganic 2D nanomaterials. So far, the shape and distribution of the as-prepared product is non-uniform, which restricts their use in fabricating devices. Chemical vapour deposition is another viable method that produces atomically thin layers of 2D metal chalcogenides on a large scale. Electrochemical methods have also been used to make thin films of metal chalcogenides. However, most of the reported literature on electrodeposition describes only the formation of different nanostructures of metal chalcogenides rather than nanosheets or nanoribbons. Therefore, as far as both physical and chemical methods are concerned, it remains a major challenge to develop new methods for the scalable production of layered inorganic nanomaterials in an easy and controlled manner.

Over the past decades, graphene, a lead material among 2D-LIN has been widely studied for gas sensing because of its high carrier mobility and low electrical noise. However, its use in real time gas sensors is limited because of its intrinsic small band gap. In recent years, new 2D-LIN such as MoS_2 and BN have attracted the attention of scientists in the gas sensor field because of their graphene like 2D layer structures, with direct band gap values.

For gas sensors, most of the reported work uses FET based devices for the detection of the gaseous species. A major challenge in developing sensors with practical application is

the development of sensors based on 2D materials with enhanced life time and improved durability. In electrochemical sensors, nanocomposites of metal chalcogenides with various novel materials needs to be explored to get good sensitivity with very low detection limit. The surface area of active materials plays a vital role in the development of sensor devices. Functionalization is often required in order to modify the surface to influence the sensing properties. The band gap of semiconducting materials can be tuned and modified by doping with noble metals such as Au, Ag, Pd and Pt. Thus, the effect of dopant on the electronic structure of the 2D inorganic materials needs to be explored further, which should lead to the introduction of enhanced features in terms of physical, chemical, electrical and optical properties. Likewise, in SERS and photodetector applications, future research lies in the development of novel nanocomposites based on 2D materials.

6 Conclusion

In this article, we have reviewed recent developments in the use of 2D layered inorganic nanomaterials such as MoS_2, WS_2, In_2S_3, SnS_2 for sensing applications. Over the last few years, graphene has attracted huge interest owing to its favourable prospects and many potential applications. However, its zero band gap limits applications in the fabrication of electronic devices like FETs, TFTs and gas sensors. Transition metal chalcogenides and inorganic layered materials are emerging as alternatives to graphene and could become novel and interesting substitutes for electronic device applications.

Acknowledgement

Authors acknowledge the support of the University Grant commission, India-UK-India Education and Research Initiative (UGC-UKIERI, Grant No. UGC-2013-14/005).

References

1 S. Guo and S. Dong, *Chem. Soc. Rev.*, 2011, **40**, 2644–2672.

2 M. I. Katsnelson, *Mater. Today*, 2007, **10**, 20–27.

3 S. Dutta and S. K. Pati, *J. Mater. Chem.*, 2010, **20**, 8207–8223.

4 K. R. Ratinac, W. Yang, S. P. Ringer and F. Braet, *Environ. Sci. Technol.*, 2010, **44**, 1167–1176.

5 C. Soldano, A. Mahmood and E. Dujardin, *Carbon N. Y.*, 2010, **48**, 2127–2150.

6 C. N. R. Rao, K. Biswas, K. S. Subrahmanyam and A. Govindaraj, *J. Mater. Chem.*, 2009, **19**, 2457–2469.

7 L.-X. Dong and Q. Chen, *Front. Mater. Sci. China*, 2010, **4**, 45–51.

8 W. Choi and J. Lee, *Graphene: synthesis and applications*, CRC Press, 2011.

9 C. N. R. Rao and A. K. Sood, *Graphene: synthesis, properties, and phenomena*, John Wiley & Sons, 2013.

10 W. Yihong, S. Zexiang and Y. Ting, *Two-Dimensional Carbon: Fundamental Properties, Synthesis, Characterization, and Applications*, CRC Press, 2014.

11 C. N. R. Rao, H. S. S. R. Matte and K. S. Subrahmanyam, *Acc. Chem. Res.*, 2012, **46**, 149–159.

12 K. Duan, Y. Du, Q. Feng, X. Ye, H. Xie, M. Xue and C. Wang, *ChemCatChem*, 2014, **6**, 1873–1876.

13 T. Wang, H. Zhu, J. Zhuo, Z. Zhu, P. Papakonstantinou, G. Lubarsky, J. Lin and M. Li, *Anal. Chem.*, 2013, **85**, 10289–10295.

14 L. Niu, K. Li, H. Zhen, Y. Chui, W. Zhang, F. Yan and Z. Zheng, *Small*, 2014, **10**, 4651–4657.

15 K. Lee, R. Gatensby, N. McEvoy, T. Hallam and G. S. Duesberg, *Adv. Mater.*, 2013, **25**, 6699–6702.

16 A. L. Friedman, F. K. Perkins, E. Cobas, G. G. Jernigan, P. M. Campbell, A. T. Hanbicki and B. T. Jonker, *Solid. State. Electron.*, 2014, **101**, 2–7.

17 Q. H. Wang, K. Kalantar-Zadeh, A. Kis, J. N. Coleman and M. S. Strano, *Nat. Nanotechnol.*, 2012, **7**, 699–712.

18 S. Wang, C. An and J. Yuan, *Materials (Basel).*, 2010, **3**, 401–433.

19 Y. Yao, Z. Lin, Z. Li, X. Song, K.-S. Moon and C. Wong, *J. Mater. Chem.*, 2012, **22**, 13494–13499.

20 X. Huang, Z. Zeng and H. Zhang, *Chem. Soc. Rev.*, 2013, **42**, 1934–1946.

21 C. N. R. Rao, H. S. S. Ramakrishna Matte and U. Maitra, *Angew. Chemie Int. Ed.*, 2013, **52**, 13162–13185.

22 X. Song, J. Hu and H. Zeng, *J. Mater. Chem. C*, 2013, **1**, 2952–2969.

23 M. Xu, T. Liang, M. Shi and H. Chen, *Chem. Rev.*, 2013, **113**, 3766–3798.

24 D. Sarkar, W. Liu, X. Xie, A. C. Anselmo, S. Mitragotri and K. Banerjee, *ACS Nano*, 2014, **8**, 3992.

25 C. N. R. Rao, K. Gopalakrishnan and U. Maitra, *ACS Appl. Mater. Interfaces*, 2015, **7**, 7809–7832.

26 C. N. R. Rao, U. Maitra and U. V Waghmare, *Chem. Phys. Lett.*, 2014, **609**, 172–183.

27 K. S. Novoselov, A. K. Geim, S. V Morozov, D. Jiang, Y. Zhang, S. V Dubonos, I. V Grigorieva and A. A. Firsov, *Science (80-.).*, 2004, **306**, 666–669.

28 D. Pacile, J. C. Meyer, C. O. Girit and A. Zettl, *Appl. Phys. Lett.*, 2008, **92**, 133107.

29 D. J. Late, *ACS Appl. Mater. Interfaces*, 2014, **6**, 1158–1163.

30 Z. Yin, H. Li, H. Li, L. Jiang, Y. Shi, Y. Sun, G. Lu, Q. Zhang, X. Chen and H. Zhang, *ACS Nano*, 2011, **6**, 74–80.

31 X. Tao and Y. Gu, *Nano Lett.*, 2013, **13**, 3501–3505.

32 N. Liu, P. Kim, J. H. Kim, J. H. Ye, S. Kim and C. J. Lee, *ACS Nano*, 2014, **8**, 6902–6910.

33 S. Yang, S. Tongay, Q. Yue, Y. Li, B. Li and F. Lu, *Sci. Rep.*, 2014, **4**.

34 H. Fang, S. Chuang, T. C. Chang, K. Takei, T. Takahashi and A. Javey, *Nano Lett.*, 2012, **12**, 3788–3792.

35 H.-U. Krebs, M. Weisheit, J. Faupel, E. Süske, T. Scharf, C. Fuhse, M. Störmer, K. Sturm, M. Seibt and H. Kijewski, in *Advances in Solid State Physics*, Springer, 2003, pp. 505–518.

36 C. W. Schneider and T. Lippert, in *Laser processing of materials*, Springer, 2010, pp. 89–112.

37 D. V Kosynkin, A. L. Higginbotham, A. Sinitskii, J. R. Lomeda, A. Dimiev, B. K. Price and J. M. Tour, *Nature*, 2009, **458**, 872–876.

38 L. Jiao, L. Zhang, X. Wang, G. Diankov and H. Dai, *Nature*, 2009, **458**, 877–880.

39 A. Hirsch, *Angew. Chemie Int. Ed.*, 2009, **48**, 6594–6596.

40 S. Ozden, P. A. S. Autreto, C. S. Tiwary, S. Khatiwada, L. Machado, D. S. Galvao, R. Vajtai, E. V Barrera and P. M. Ajayan, *Nano Lett.*, 2014, **14**, 4131–4137.

41 M. Terrones, *ACS Nano*, 2010, **4**, 1775–1781.

42 H. Santos, L. Chico and L. Brey, *Phys. Rev. Lett.*, 2009, **103**, 86801.

43 A. Sinitskii, A. A. Fursina, D. V Kosynkin, A. L. Higginbotham, D. Natelson and J. M. Tour, *Appl. Phys. Lett.*, 2009, **95**, 253108.

44 S. Mohammadi, Z. Kolahdouz, S. Darbari, S. Mohajerzadeh and N. Masoumi, *Carbon N. Y.*, 2013, **52**, 451–463.

45 R. Pelalak, M. Baniadam and M. Maghrebi, *Appl. Phys. A*, 2013, **111**, 951–957.

46 D. B. Shinde, J. Debgupta, A. Kushwaha, M. Aslam and V. K. Pillai, *J. Am. Chem. Soc.*, 2011, **133**, 4168–4171.

47 P. Kumar, L. S. Panchakarla and C. N. R. Rao, *Nanoscale*, 2011, **3**, 2127–2129.

48 S. Ding, D. Zhang, J. S. Chen and X. W. D. Lou, *Nanoscale*, 2012, **4**, 95–98.

49 J. Yang, D. Voiry, S. J. Ahn, D. Kang, A. Y. Kim, M. Chhowalla and H. S. Shin, *Angew. Chemie Int. Ed.*, 2013, **52**, 13751–13754.

50 H. Zhu, D. Yang, Y. Ji, H. Zhang and X. Shen, *J. Mater. Sci.*, 2005, **40**, 591–595.

51 J. Feng, X. Sun, C. Wu, L. Peng, C. Lin, S. Hu, J. Yang and Y. Xie, *J. Am. Chem. Soc.*, 2011, **133**, 17832–17838.

52 W. Dong, X. Wang, B. Li, L. Wang, B. Chen, C. Li, X. Li, T. Zhang and Z. Shi, *Dalt. Trans.*, 2011, **40**, 243–248.

53 B. Saravanakumar and S. J. Kim, *J. Phys. Chem. C*, 2014.

54 C. Wang, J. Xu, M. Yuen, J. Zhang, Y. Li, X. Chen and W. Zhang, *Adv. Funct. Mater.*, 2014, **24**, 6372–6380.

55 J. Wang, B. Gao, L. Zhang, R. Li, J. Shen, Z. Qiao, G. Yang and F. Nie, *RSC Adv.*, 2014, **4**, 30573–30578.

56 J. He, H. Liu, B. Xu and X. Wang, *Small*, 2014.

57 H. Cheng, T. Kamegawa, K. Mori and H. Yamashita, *Angew. Chemie Int. Ed.*, 2014, **53**, 2910–2914.

58 R. Ma, Y. Bando, L. Zhang and T. Sasaki, *Adv. Mater.*, 2004, **16**, 918–922.

59 S. Ji, Z. Yang, C. Zhang, Z. Liu, W. W. Tjiu, I. Y. Phang, Z. Zhang, J. Pan and T. Liu, *Electrochim. Acta*, 2013, **109**, 269–275.

60 V. H. Pham, K.-H. Kim, D.-W. Jung, K. Singh, E.-S. Oh and J. S. Chung, *J. Power Sources*, 2013, **244**, 280–286.

61 Y. Wang, Z. Shi and J. Yin, *J. Mater. Chem.*, 2011, **21**, 11371–11377.

62 S.-L. Zhang, H.-H. Choi, H.-Y. Yue and W.-C. Yang, *Curr. Appl. Phys.*, 2014, **14**, 264–268.

63 J. Huang, Y. He, J. Jin, Y. Li, Z. Dong and R. Li, *Electrochim. Acta*, 2014, **136**, 41–46.

64 A. Winchester, S. Ghosh, S. Feng, A. L. Elias, T. Mallouk, M. Terrones and S. Talapatra, *ACS Appl. Mater. Interfaces*, 2014, **6**, 2125–2130.

65 J. J. Devadasan, C. Sanjeeviraja and M. Jayachandran, *J. Cryst. Growth*, 2001, **226**, 67–72.

66 B. Chakraborty, B. Show, S. Jana, B. C. Mitra, S. K. Maji, B. Adhikary, N. Mukherjee and A. Mondal, *Electrochim. Acta*, 2013, **94**, 7–15.

67 Y. Chen, C. Davoisne, J.-M. Tarascon and C. Guéry, *J. Mater. Chem.*, 2012, **22**, 5295–5299.

68 N. R. Mathews, H. B. M. Anaya, M. A. Cortes-Jacome, C. Angeles-Chavez and J. A. Toledo-Antonio, *J. Electrochem. Soc.*, 2010, **157**, H337–H341.

69 Y.-M. Yeh, H. Chen, C. Wang and C. H. Liao, *Thin Solid Films*, 2013, **529**, 103–106.

70 M. M. Arafat, B. Dinan, S. A. Akbar and A. Haseeb, *Sensors*, 2012, **12**, 7207–7258.

71 J. Huang and Q. Wan, *Sensors*, 2009, **9**, 9903–9924.

72 T. Ahuja and D. Kumar, *Sensors Actuators B Chem.*, 2009, **136**, 275–286.

73 *J. Mater. Chem. A*, 2013, **1**, 10078.

74 Y. Wang and J. T. W. Yeow, *J. Sensors*, 2009, **2009**.

75 B. Liu, L. Chen, G. Liu, A. N. Abbas, M. Fathi and C. Zhou, *ACS Nano*, 2014, **8**, 5304–5314.

76 B. Cho, M. G. Hahm, M. Choi, J. Yoon, A. R. Kim, Y.-J. Lee, S.-G. Park, J.-D. Kwon, C. S. Kim, M. Song, Y. Jeong, K.-S. Nam, S. Lee, T. J. Yoo, C. G. Kang, B. H. Lee, H. C. Ko, P. M. Ajayan and D.-H. Kim, *Sci. Rep.*, 2015, **5**.

77 A. Tricoli, M. Righettoni and A. Teleki, *Angew. Chemie Int. Ed.*, 2010, **49**, 7632–7659.

78 S. M. Kanan, O. M. El-Kadri, I. A. Abu-Yousef and M. C. Kanan, *Sensors*, 2009, **9**, 8158–8196.

79 H. Bai and G. Shi, *Sensors*, 2007, **7**, 267–307.

80 S. Basu and P. Bhattacharyya, *Sensors Actuators B Chem.*, 2012, **173**, 1–21.

81 F. Yavari and N. Koratkar, *J. Phys. Chem. Lett.*, 2012, **3**, 1746–1753.

82 B. Reddy, *Advances in nanocomposites-Synthesis, characterization and industrial applications*, InTech Rijeka, Croatia, 2011.

83 S. Some, Y. Xu, Y. Kim, Y. Yoon, H. Qin, A. Kulkarni, T. Kim and H. Lee, *Sci. Rep.*, 2013, **3**.

84 N. Peng, Q. Zhang, Y. C. Lee, O. K. Tan and N. Marzari, *Sensors Actuators B Chem.*, 2008, **132**, 191–195.

85 E. Gourmelon, O. Lignier, H. Hadouda, G. Couturier, J. C. Bernède, J. Tedd, J. Pouzet and J. Salardenne, *Sol. Energy Mater. Sol. Cells*, 1997, **46**, 115–121.

86 E. Fortin and W. M. Sears, *J. Phys. Chem. Solids*, 1982, **43**, 881–884.

87 R. Gatensby, N. McEvoy, K. Lee, T. Hallam, N. C. Berner, E. Rezvani, S. Winters, M. O'Brien and G. S. Duesberg, *Appl. Surf. Sci.*, 2014, **297**, 139–146.

88 W. Shi, L. Huo, H. Wang, H. Zhang, J. Yang and P. Wei, *Nanotechnology*, 2006, **17**, 2918.

89 F. K. Perkins, A. L. Friedman, E. Cobas, P. M. Campbell, G. G. Jernigan and B. T. Jonker, *Nano Lett.*, 2013, **13**, 668–673.

90 Q. He, Z. Zeng, Z. Yin, H. Li, S. Wu, X. Huang and H. Zhang, *Small*, 2012, **8**, 2994–2999.

91 D. J. Late, Y.-K. Huang, B. Liu, J. Acharya, S. N. Shirodkar, J. Luo, A. Yan, D. Charles, U. V Waghmare and V. P. Dravid, *ACS Nano*, 2013, **7**, 4879–4891.

92 J.-S. Kim, H.-W. Yoo, H. O. Choi and H.-T. Jung, *Nano Lett.*, 2014, **14**, 5941–5947.

93 C.-Z. HU, F. LI and X.-D. LIU, *Acta Chim. Sin.*, 2008, **66**, 1641.

94 Y. Xie, Y.-P. Huo and J.-M. Zhang, *Appl. Surf. Sci.*, 2012, **258**, 6391–6397.

95 A. Soltani, S. G. Raz, V. J. Rezaei, A. D. Khalaji and M. Savar, *Appl. Surf. Sci.*, 2012, **263**, 619–625.

96 P. Singla, S. Singhal and N. Goel, *Appl. Surf. Sci.*, 2013, **283**, 881–887.

97 P. Srivastava, N. K. Jaiswal and V. Sharma, *Superlattices Microstruct.*, 2014, **73**, 350–358.

98 A. Srivastava, C. Bhat, S. K. Jain, P. K. Mishra and R. Brajpuriya, *J. Mol. Model.*, 2015, **21**, 1–8.

99 M. Sajjad and P. Feng, *Mater. Res. Bull.*, 2014, **49**, 35–38.

100 L. Chen, B. Liu and C. Zhou, *Bull. Am. Phys. Soc.*, 2014.

101 D. Wang, K. Zhou, M. Sun, Z. Fang, X. Liu and X. Sun, *Anal. Methods*, 2013, **5**, 6576–6578.

102 A. Umar, M. S. Akhtar, G. N. Dar, M. Abaker, A. Al-Hajry and S. Baskoutas, *Talanta*, 2013, **114**, 183–190.

103 J. Feng, L. Peng, C. Wu, X. Sun, S. Hu, C. Lin, J. Dai, J. Yang and Y. Xie, *Adv. Mater.*, 2012, **24**, 1969–1974.

104 C. Zhu, G. Yang, H. Li, D. Du and Y. Lin, *Anal. Chem.*, 2015.

105 J. P. Metters and C. E. Banks, *Nanomater. Electrochem. Sens. Biosensing*, 2014, 1.

106 S. Guo and E. Wang, *Nano Today*, 2011, **6**, 240–264.

107 J. G. M. Santos, J. R. Souza, C. J. Letti, M. A. G. Soler, P. C. Morais, M. A. Pereira-da-Silva and L. G. Paterno, *J. Nanosci. Nanotechnol.*, 2014, **14**, 6614–6623.

108 M. Mazloum-Ardakani, M. A. Sheikh-Mohseni and M. Abdollahi-Alibeik, *J. Mol. Liq.*, 2013, **178**, 63–69.

109 Q. Zhao, Z. Gan and Q. Zhuang, *Electroanalysis*, 2002, **14**, 1609–1613.

110 T. Gan and S. Hu, *Microchim. Acta*, 2011, **175**, 1–19.

111 S. R. Ali, Y. Ma, R. R. Parajuli, Y. Balogun, W. Y.-C. Lai and H. He, *Anal. Chem.*, 2007, **79**, 2583–2587.

112 S. Chandra, H. Lang and D. Bahadur, *Anal. Chim. Acta*, 2013, **795**, 8–14.

113 M. Lin, *RSC Adv.*, 2015, **5**, 9848–9851.

114 B. Šljukic, C. E. Banks and R. G. Compton, *Nano Lett.*, 2006, **6**, 1556–1558.

115 H. Teymourian, A. Salimi and S. Khezrian, *Biosens. Bioelectron.*, 2013, **49**, 1–8.

116 F. Xu, Y. Sun, Y. Zhang, Y. Shi, Z. Wen and Z. Li, *Electrochem. commun.*, 2011, **13**, 1131–1134.

117 R. Zhang and X. Wang, *Chem. Mater.*, 2007, **19**, 976–978.

118 Y. Zhao, X. Fang, Y. Gu, X. Yan, Z. Kang, X. Zheng, P. Lin, L. Zhao and Y. Zhang, *Colloids Surfaces B Biointerfaces*, 2015.

119 L. Zhou, Q. Yuan, X. Li, J. Xu, F. Xia and J. Xiao, *Sensors Actuators B Chem.*, 2015, **206**, 311–318.

120 Z. Zhuang, J. Li, R. Xu and D. Xiao, *Int. J. Electrochem. Sci*, 2011, **6**, 2149–2161.

121 S. Wu, Z. Zeng, Q. He, Z. Wang, S. J. Wang, Y. Du, Z. Yin, X. Sun, W. Chen and H. Zhang, *Small*, 2012, **8**, 2264–2270.

122 K.-J. Huang, L. Wang, Y.-J. Liu, T. Gan, Y.-M. Liu, L.-L. Wang and Y. Fan, *Electrochim. Acta*, 2013.

123 J. Li, Z. Yang, Y. Tang, Y. Zhang and X. Hu, *Biosens. Bioelectron.*, 2013, **41**, 698–703.

124 T.-W. Lin, C.-J. Liu and C.-S. Dai, *Appl. Catal. B Environ.*, 2014, **154–155**, 213–220.

125 H. Sun, J. Chao, X. Zuo, S. Su, X. Liu, L. Yuwen, C. Fan and L. Wang, *RSC Adv.*, 2014, **4**, 27625–27629.

126 S. Su, H. Sun, F. Xu, L. Yuwen and L. Wang, *Electroanalysis*, 2013, **25**, 2523–2529.

127 J. Li, Z. Yang, Y. Zhang, S. Yu, Q. Xu, Q. Qu and X. Hu, *Microchim. Acta*, 2012, **179**, 265–272.

128 K.-J. Huang, Y.-J. Liu, Y.-M. Liu and L.-L. Wang, *J. Hazard. Mater.*, 2014.

129 X. Xia, Z. Zheng, Y. Zhang, X. Zhao and C. Wang, *Sensors Actuators B Chem.*, 2014, **192**, 42–50.

130 J. Huang, Z. Dong, Y. Li, J. Li, W. Tang, H. Yang, J. Wang, Y. Bao, J. Jin and R. Li, *Mater. Res. Bull.*, 2013, **48**, 4544–4547.

131 S. Virji, J. Huang, R. B. Kaner and B. H. Weiller, *Nano Lett.*, 2004, **4**, 491–496.

132 L. Yang, W. Qiu and Q. Liu, *Solid State Ionics*, 1996, **86**, 819–824.

133 Y.-E. Miao, W. Fan, D. Chen and T. Liu, *ACS Appl. Mater. Interfaces*, 2013, **5**, 4423–4428.

134 J. Fang, K. Xu, L. Zhu, Z. Zhou and H. Tang, *Corros. Sci.*, 2007, **49**, 4232–4242.

135 K.-J. Huang, J.-Z. Zhang, Y.-J. Liu and L.-L. Wang, *Sensors Actuators B Chem.*, 2014, **194**, 303–310.

136 K.-J. Huang, L. Wang, J. Li and Y.-M. Liu, *Sensors Actuators B Chem.*, 2013, **178**, 671–677.

137 Q. Feng, K. Duan, X. Ye, D. Lu, Y. Du and C. Wang, *Sensors Actuators B Chem.*, 2014, **192**, 1–8.

138 D. Grieshaber, R. MacKenzie, J. Voeroes and E. Reimhult, *Sensors*, 2008, **8**, 1400–1458.

139 H. Song, Y. Ni and S. Kokot, *Biosens. Bioelectron.*, 2014, **56**, 137–143.

140 A. Matsumoto and Y. Miyahara, *Nanoscale*, 2013, **5**, 10702–10718.

141 T. N. Narayanan, C. S. R. Vusa and S. Alwarappan, *Nanotechnology*, 2014, **25**, 335702.

142 S. Wu, G. Liu, P. Li, H. Liu and H. Xu, *Biosens. Bioelectron.*, 2012, **38**, 289–294.

143 G.-X. Wang, W.-J. Bao, J. Wang, Q.-Q. Lu and X.-H. Xia, *Electrochem. commun.*, 2013, **35**, 146–148.

144 K.-J. Huang, Y.-J. Liu, H.-B. Wang, Y.-Y. Wang and Y.-M. Liu, *Biosens. Bioelectron.*, 2014, **55**, 195–202.

145 S. Su, H. Sun, F. Xu, L. Yuwen, C. Fan and L. Wang, *Microchim. Acta*, 2014, 1–7.

146 Y. Pan, Y. Zhang and Y. Li, *J. Appl. Polym. Sci.*, 2013, **128**, 647–652.

147 K.-J. Huang, Y.-J. Liu, H.-B. Wang, T. Gan, Y.-M. Liu and L.-L. Wang, *Sensors Actuators B Chem.*, 2014, **191**, 828–836.

148 H. Liu, X. Su, C. Duan, X. Dong and Z. Zhu, *Mater. Lett.*, 2014, **122**, 182–185.

149 S. Schlücker, *Angew. Chemie Int. Ed.*, 2014, **53**, 4756–4795.

150 B. Sharma, R. R. Frontiera, A.-I. Henry, E. Ringe and R. P. Van Duyne, *Mater. today*, 2012, **15**, 16–25.

151 G. McNay, D. Eustace, W. E. Smith, K. Faulds and D. Graham, *Appl. Spectrosc.*, 2011, **65**, 825–837.

152 R. A. Halvorson and P. J. Vikesland, *Environ. Sci. Technol.*, 2010, **44**, 7749–7755.

153 K. Hering, D. Cialla, K. Ackermann, T. Dörfer, R. Möller, H. Schneidewind, R. Mattheis, W. Fritzsche, P. Rösch and J. Popp, *Anal. Bioanal. Chem.*, 2008, **390**, 113–124.

154 X. Ling, W. Fang, Y.-H. Lee, P. T. Araujo, X. Zhang, J. F. Rodriguez-Nieva, Y. Lin, J. Zhang, J. Kong and M. S. Dresselhaus, *Nano Lett.*, 2014, **14**, 3033–3040.

155 K. L. Kelly, E. Coronado, L. L. Zhao and G. C. Schatz, *J. Phys. Chem. B*, 2003, **107**, 668–677.

156 A. Otto, I. Mrozek, H. Grabhorn and W. Akemann, *J. Phys. Condens. Matter*, 1992, **4**, 1143.

157 L. Baia, L. Diamandescu, L. Barbu-Tudoran, A. Peter, G. Melinte, V. Danciu and M. Baia, *J. Alloys Compd.*, 2011, **509**, 2672–2678.

158 L. Sun, H. Hu, D. Zhan, J. Yan, L. Liu, J. S. Teguh, E. K. L. Yeow, P. S. Lee and Z. Shen, *Small*, 2014, **10**, 1090–1095.

159 J. Zhao, Z. Zhang, S. Yang, H. Zheng and Y. Li, *J. Alloys Compd.*, 2013, **559**, 87–91.

160 T. Zhai, L. Li, X. Wang, X. Fang, Y. Bando and D. Golberg, *Adv. Funct. Mater.*, 2010, **20**, 4233–4248.

161 F. H. L. Koppens, T. Mueller, P. Avouris, A. C. Ferrari, M. S. Vitiello and M. Polini, *Nat. Nanotechnol.*, 2014, **9**, 780–793.

162 Z. Alaie, S. M. Nejad and M. H. Yousefi, *Mater. Sci. Semicond. Process.*, 2015, **29**, 16–55.

163 D. Choi, Y. Jang, J. Lee, G. H. Jeong, D. Whang, S. W. Hwang, K.-S. Cho and S.-W. Kim, *Sci. Rep.*, 2014, **4**.

164 T. J. Echtermeyer, L. Britnell, P. K. Jasnos, A. Lombardo, R. V Gorbachev, A. N. Grigorenko, A. K. Geim, A. C. Ferrari and K. S. Novoselov, *Nat. Commun.*, 2011, **2**, 458.

165 Y. Liu, R. Cheng, L. Liao, H. Zhou, J. Bai, G. Liu, L. Liu, Y. Huang and X. Duan, *Nat. Commun.*, 2011, **2**, 579.

166 M. Furchi, A. Urich, A. Pospischil, G. Lilley, K. Unterrainer, H. Detz, P. Klang, A. M. Andrews, W. Schrenk and G. Strasser, *Nano Lett.*, 2012, **12**, 2773–2777.

167 P. Hu, Z. Wen, L. Wang, P. Tan and K. Xiao, *ACS Nano*, 2012, **6**, 5988–5994.

168 S. H. Yu, Y. Lee, S. K. Jang, J. Kang, J. Jeon, C. Lee, J. Y. Lee, H. Kim, E. Hwang and S. Lee, *ACS Nano*, 2014, **8**, 8285–8291.

169 K. Roy, M. Padmanabhan, S. Goswami, T. P. Sai, G. Ramalingam, S. Raghavan and A. Ghosh, *Nat. Nanotechnol.*, 2013, **8**, 826–830.

170 J. O. Island, M. Buscema, M. Barawi, J. M. Clamagirand, J. R. Ares, C. Sánchez, I. J. Ferrer, G. A. Steele, H. S. J. van der Zant and A. Castellanos-Gomez, *Adv. Opt. Mater.*, 2014.

171 S. Lei, L. Ge, Z. Liu, S. Najmaei, G. Shi, G. You, J. Lou, R. Vajtai and P. M. Ajayan, *Nano Lett.*, 2013, **13**, 2777–2781.

172 P. Hu, L. Wang, M. Yoon, J. Zhang, W. Feng, X. Wang, Z. Wen, J. C. Idrobo, Y. Miyamoto and D. B. Geohegan, *Nano Lett.*, 2013, **13**, 1649–1654.

173 X. Li, M.-W. Lin, A. A. Puretzky, J. C. Idrobo, C. Ma, M. Chi, M. Yoon, C. M. Rouleau, I. I. Kravchenko and D. B. Geohegan, *Sci. Rep.*, 2014, **4**.

174 N. Drummond, V. I. Fal'ko and K. Tanigaki, 2013.

175 T. R. Srinivasa, Y.-Y. Lu, R. K. U, R. Sankar, C.-D. Liao, C.-H. Cheng, F. C. Chou and Y.-T. Chen, *Nano Lett.*, 2014.

176 Y. Yu, Y. Jiang, K. Zheng, Z. Zhu, X. Lan, Y. Zhang, Y. Zhang and X. Xuan, *J. Mater. Chem. C*, 2014, **2**, 3583–3588.

177 D. Xiang, C. Han, J. Zhang and W. Chen, *Sci. Rep.*, 2014, **4**.